地球惑星観測・探査学／惑星探査学2
「宇宙機を用いた電波観測」
Radio observations of planets using spacecraft

新領域創成科学研究科　複雑理工学専攻
今村　剛
Takeshi Imamura

Merit of radio observation

- Techniques of high-precision frequency measurements are available. This enables accurate retrieval of atmospheric structures.
- Facilities for telecommunication can be used for observations. This saves weight resources of spacecraft.

- Two types of observations are considered in today's talk
  - Radio occultation (active method)
  - Spectroscopy/radiometer (passive method)

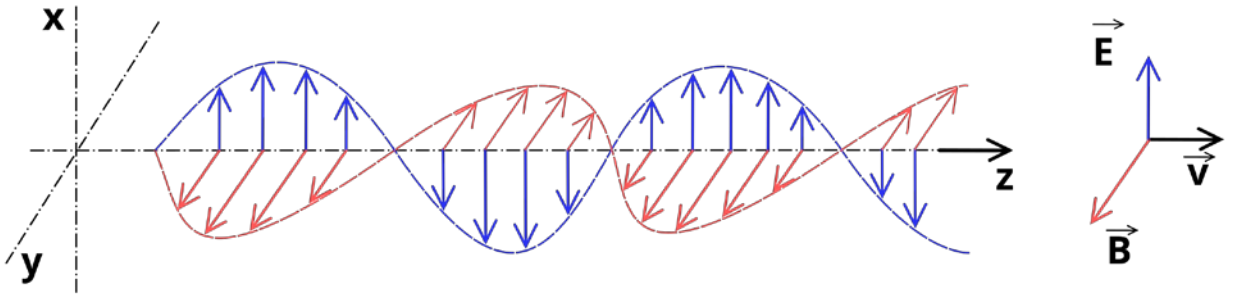

from Wikipedia

Vertical temperature profiles of planetary atmospheres

(Mueller-Wodarg et al.)

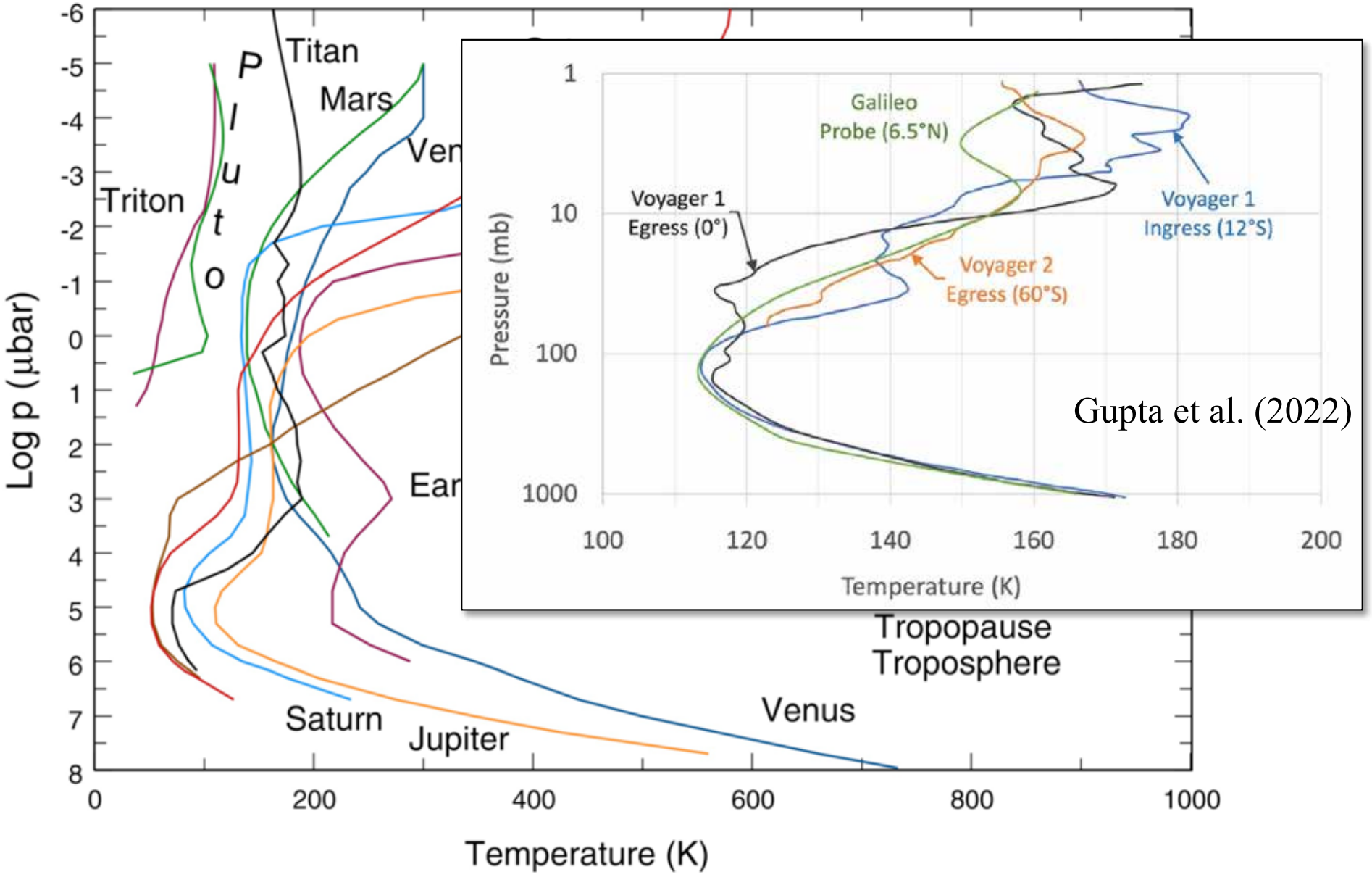

Radio occultation (電波掩蔽)

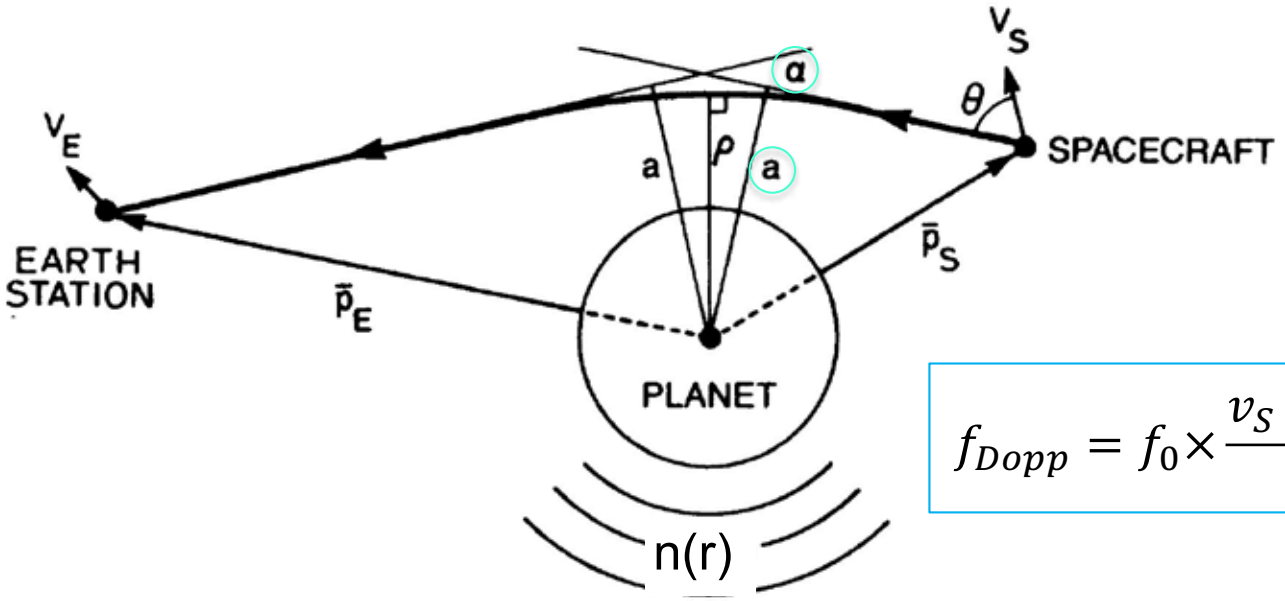

$$f_{Dopp} = f_0 \times \frac{v_S \cos\theta}{c}$$

a : Impact parameter
α : Bending angle
n : Refractive index
r : Distance from planet center

Tyler (1987)

Abel transformation:

$$\ln n(r) = -\frac{1}{\pi}\int_{a_1}^{\infty} \ln\left\{\frac{a}{a_1} + \left[\left(\frac{a}{a_1}\right)^2 - 1\right]^{\frac{1}{2}}\right\}\frac{d\alpha}{da}da$$

$n(r)\, r = a$ a : Impact parameter for a ray whose radius of closest approach is r

Ultra-Stable Oscillator (USO) on Venus orbiter Akatsuki

Stability of USO after the launch

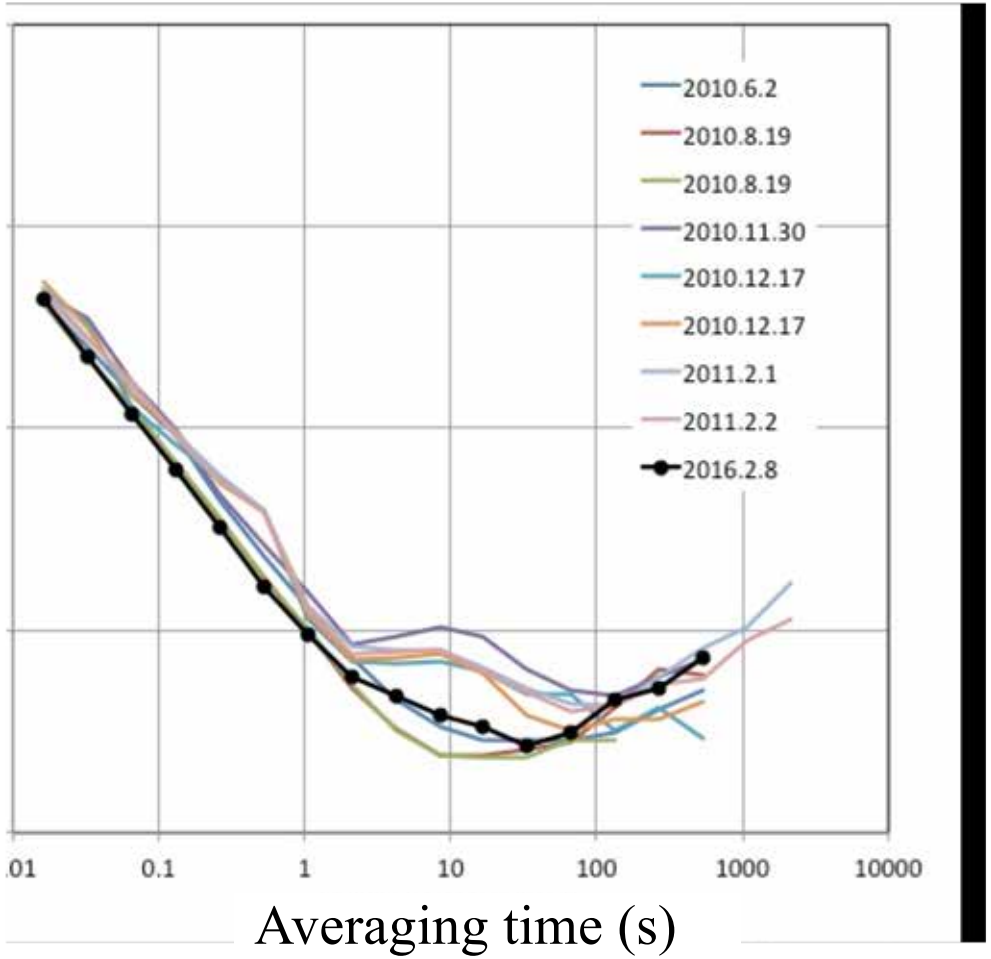

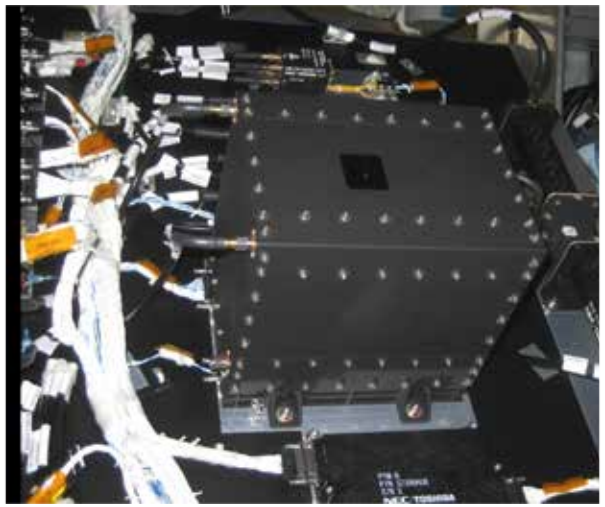

USO on Akatsuki

The requirement (Allan dev $< 1 \times 10^{-12}$ for τ = 1-1000 s) is satisfied.

High-gain antenna

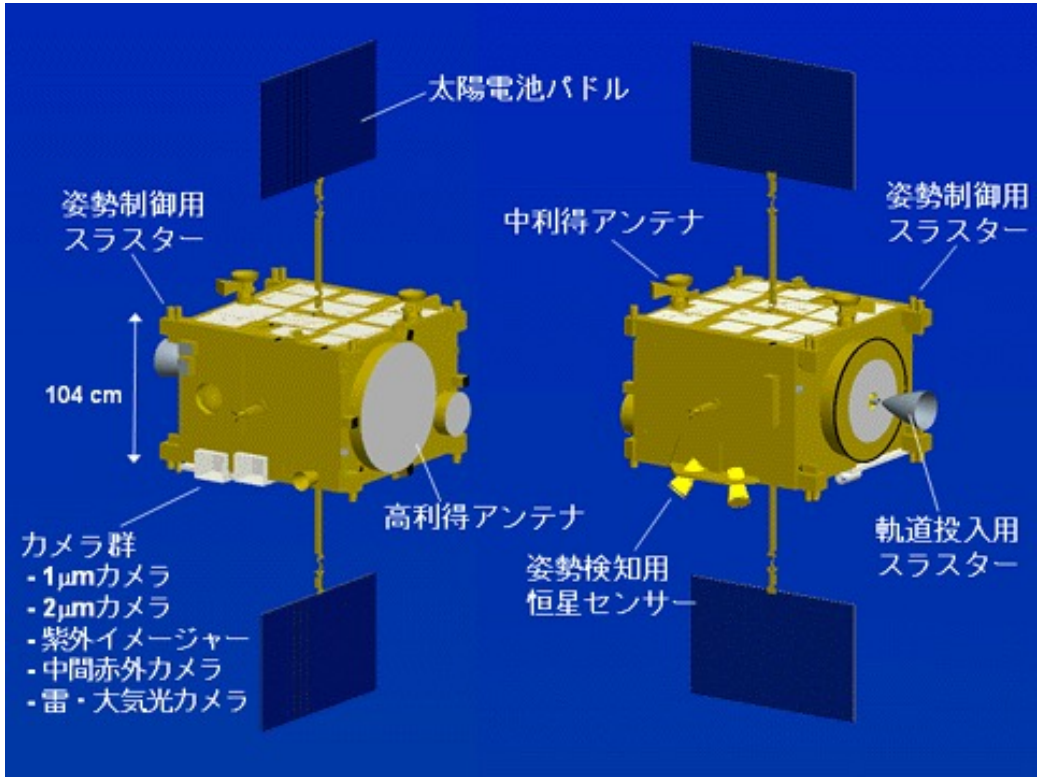

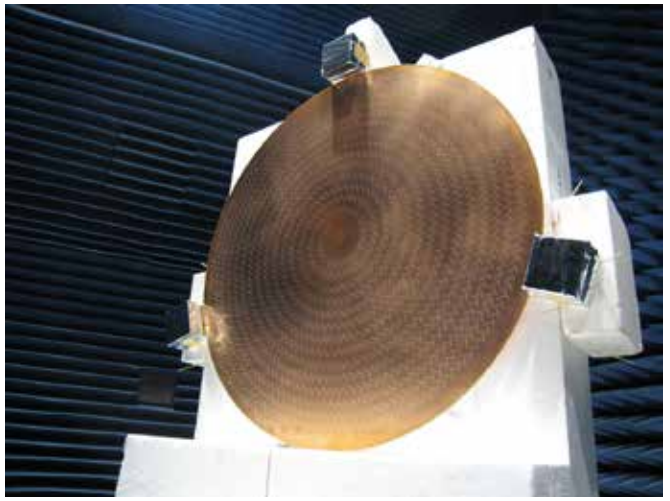

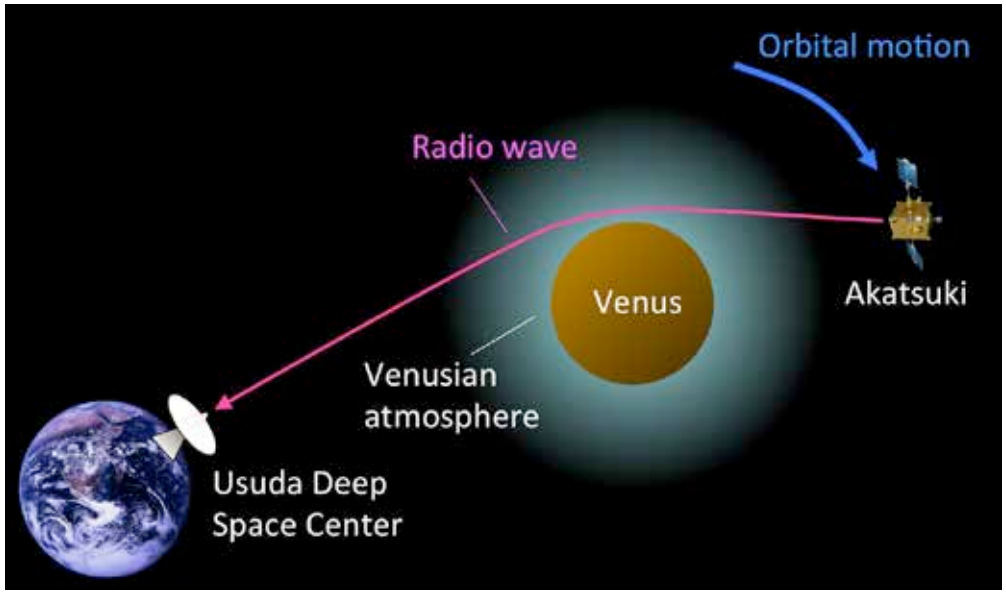

Attitude maneuver is needed during experiments due to ray bending

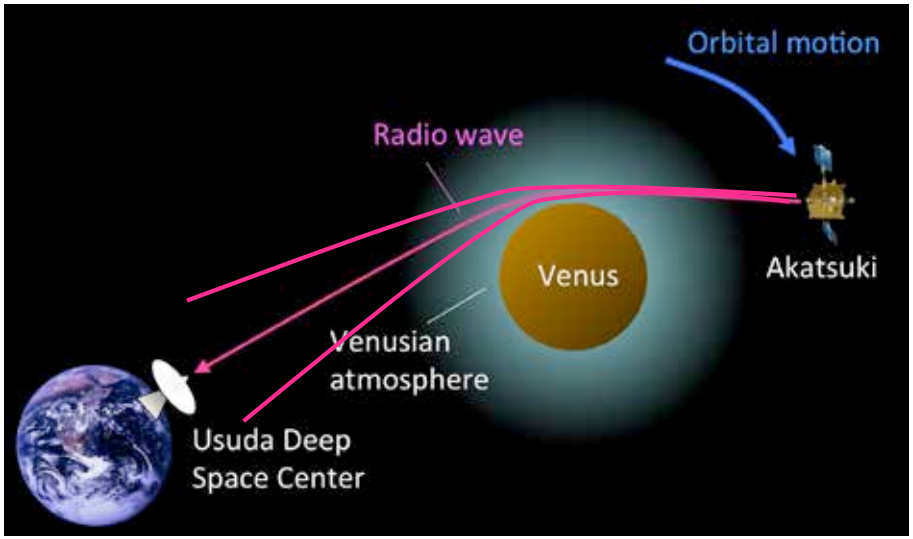

Signal intensity time series (example from Akatsuki)

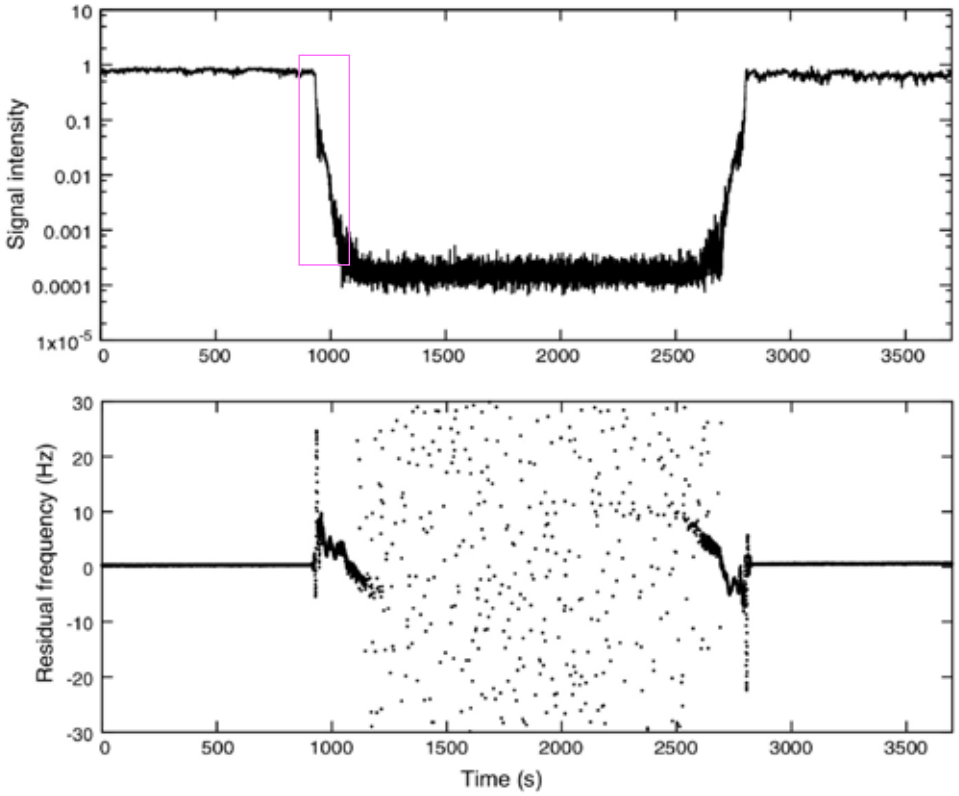

Defocusing loss

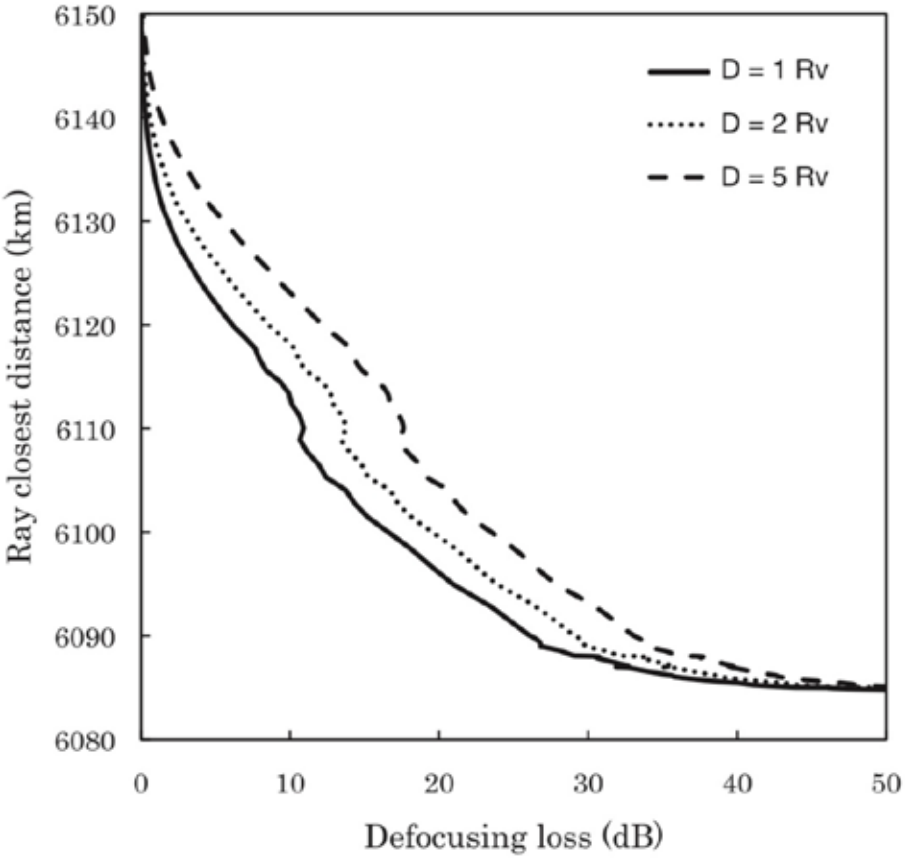

Data acquisition

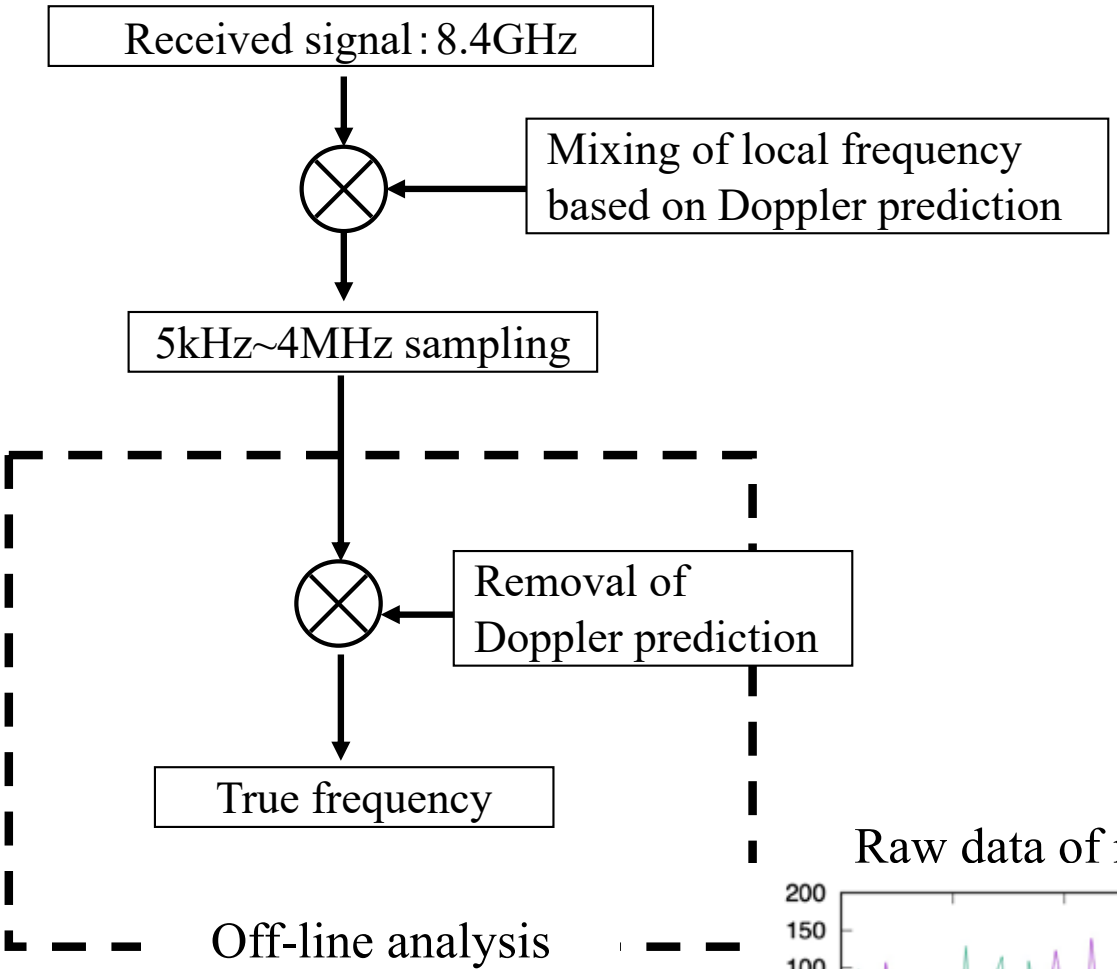

Usuda Deep Space Center (UDSC)

Raw data of radio wave from Venus orbiter Akatsuki

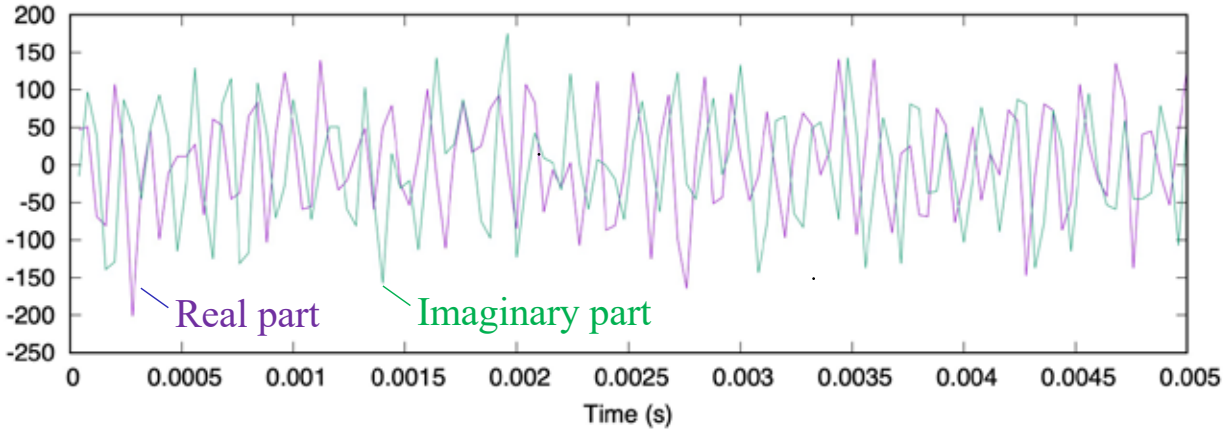

Need for narrow-band filtering (example from Akatsuki)

- Signal level at the receiver: $P = 3.0 \times 10^{-17}$ W (at 1.73 × Earth-Sun-distance)
- Noise temperature of the receiver = 96 K (Usuda Deep Space Center, Japan)

  → $kT \sim 1.3 \times 10^{-21}$ (unit: J = W/Hz)

Letting the band width be B (Hz), the S/N ratio is given by

$$P / kTB \sim 2.3 \times 10^{-4} / B$$

So that the S/N ratio is higher than the required value of ~10000, we require

$$B < 20 \text{ Hz}$$

Signal spectrum

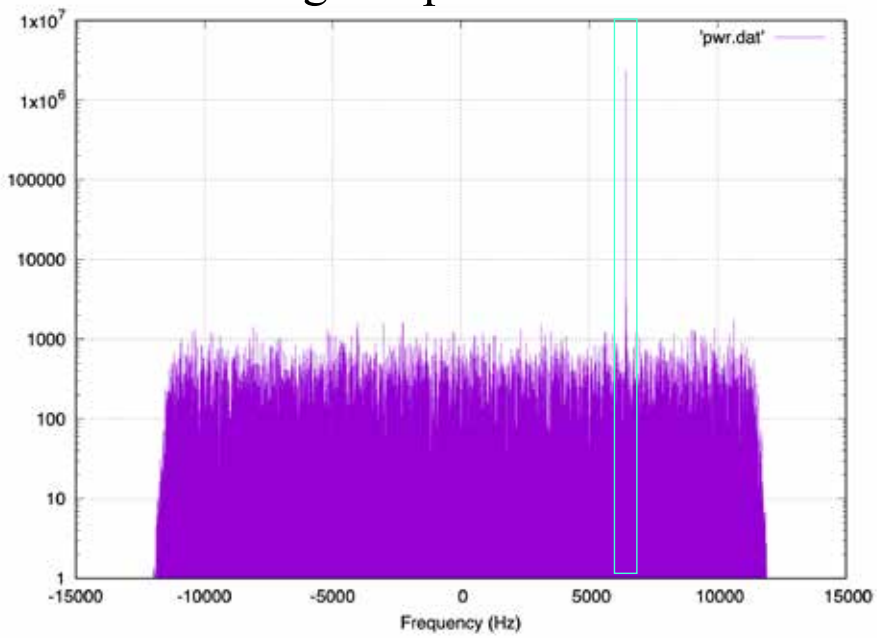

Filtering and decimation

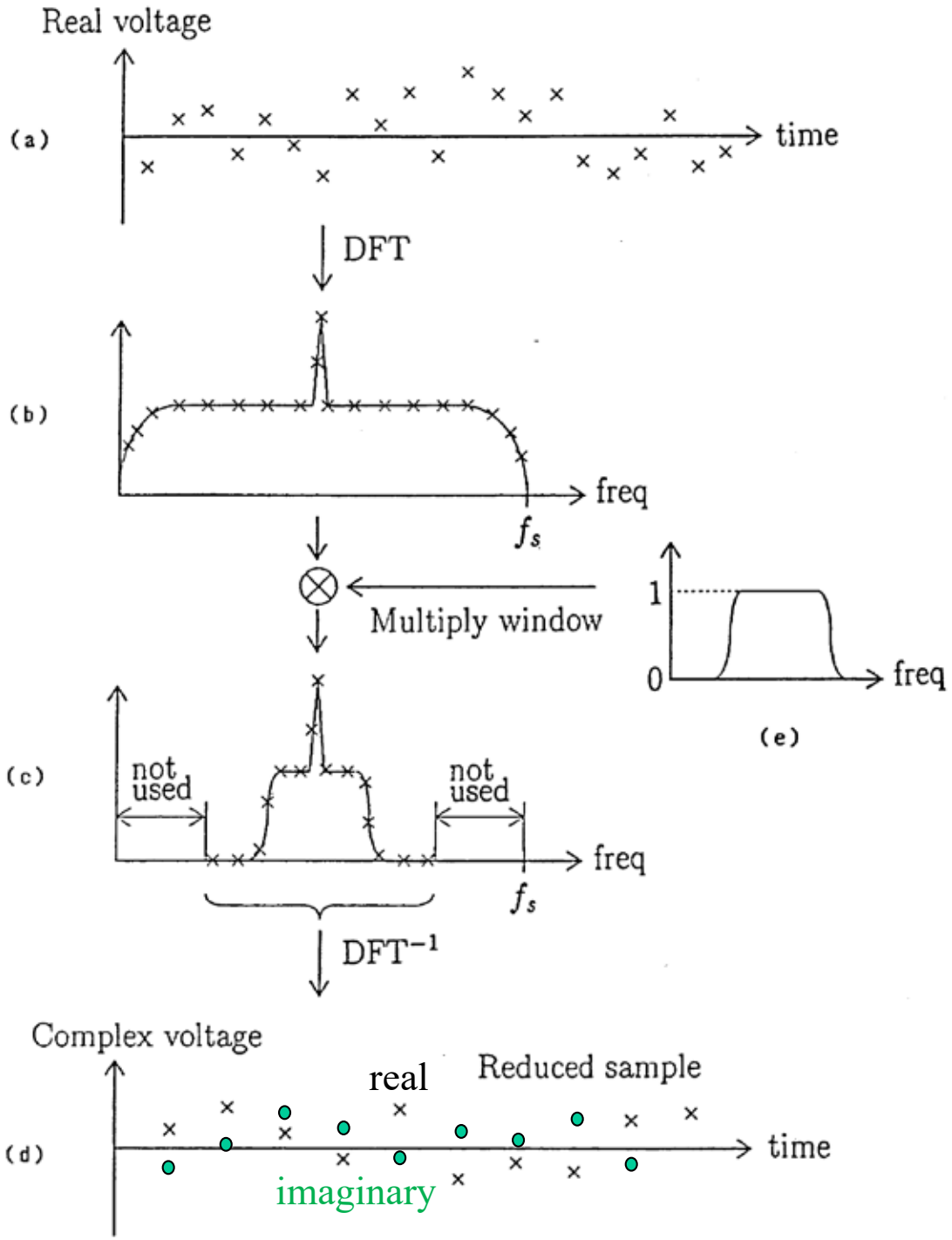

Precise phase/frequency estimation by phase unwrapping

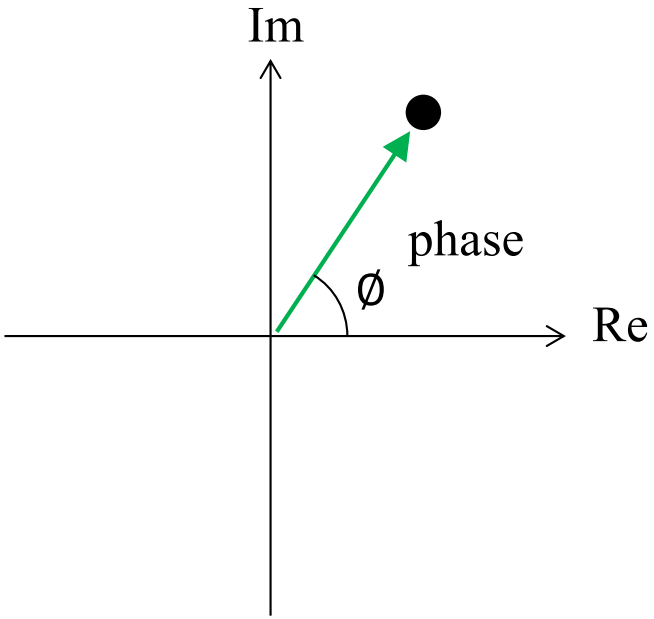

frequency : $f = \frac{d\emptyset}{dt}$

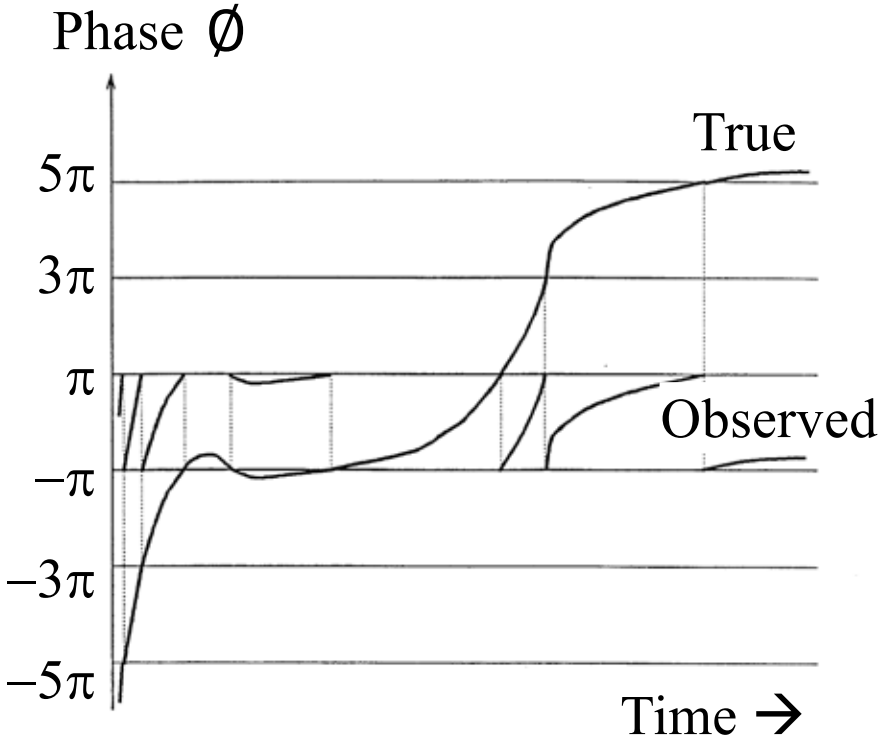

With sufficiently low-noise, the phase can be obtained from the real and imaginary components of the data at each time step. The frequency is obtained by differentiating the phase.

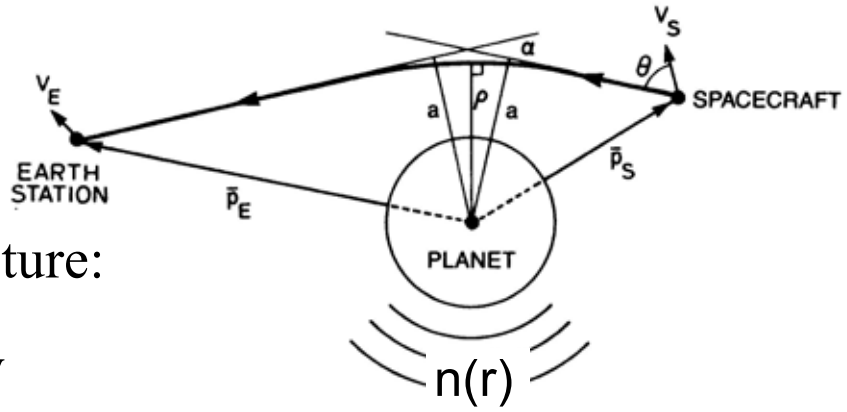

Refractive index n is related to atmospheric structure:

$$\mu(r) = (n(r) - 1) \times 10^6 \qquad \text{: Refractivity}$$

$$= \kappa N_n(r) - 40.3 \frac{N_e(r)}{f_0^2} \times 10^6$$

neutral atmosphere

plasma

Retrieval of the neutral atmosphere's temperature based on hydrostatic equilibrium:

$$T(r) = \frac{N_n(r_{top})}{N_n(r)} T(r_{top}) + \frac{\overline{m}}{k N_n(r)} \int_r^{r_{top}} N_n(r') g(r') dr$$

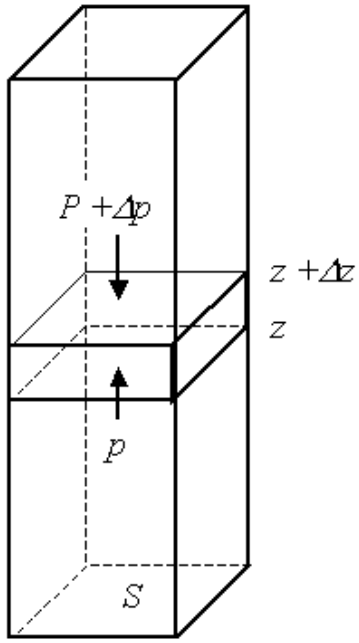

$$-S\Delta p = g\rho S\Delta z$$

$$\therefore \frac{dp}{dz} = -g\rho$$

Temperature at the upper boundary should be given from empirical models. The effect of the upper boundary almost disappears 1-2 scale heights below the boundary.

Retrieval of a temperature profile

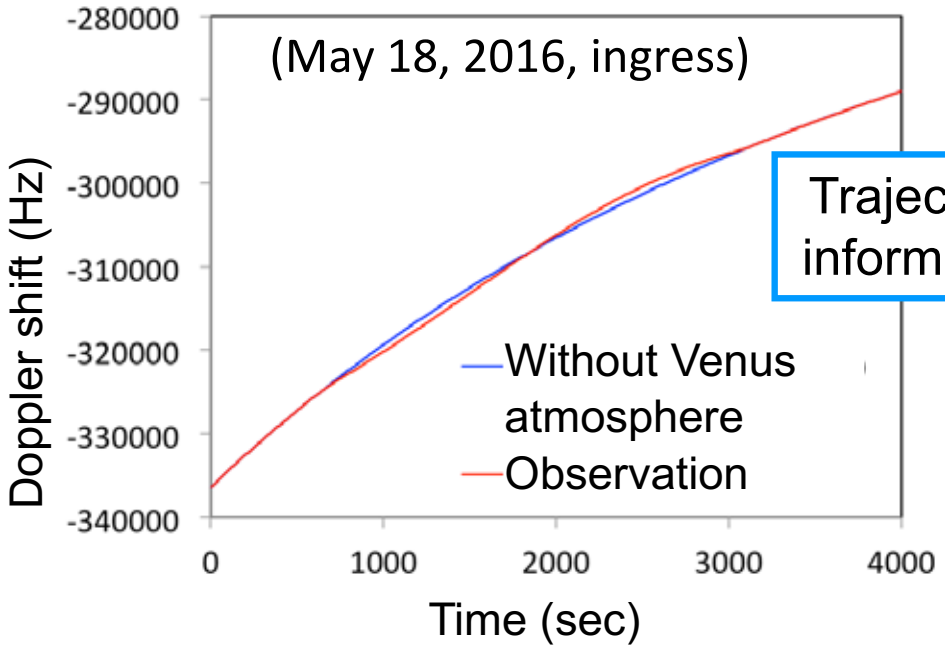

Trajectory information

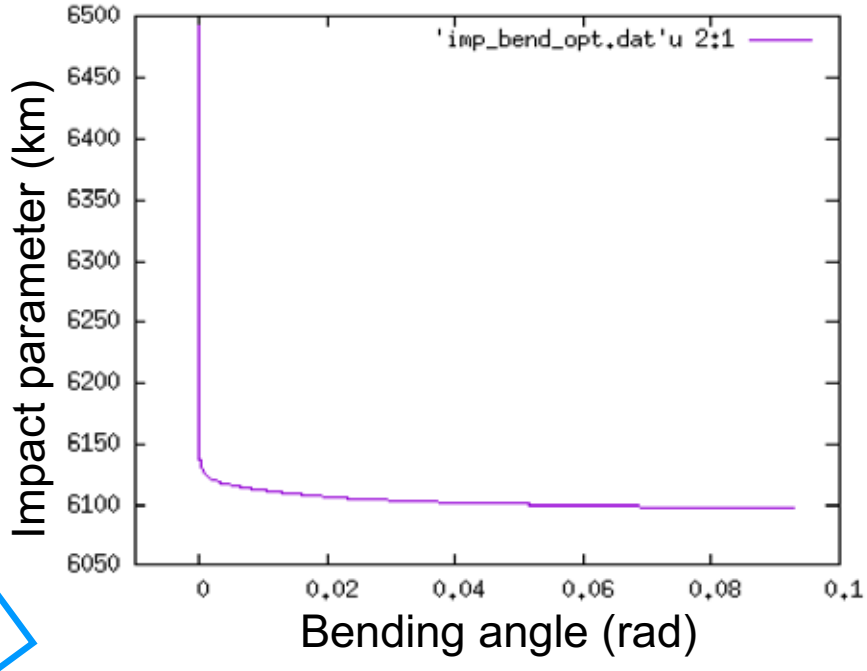

Abel transform

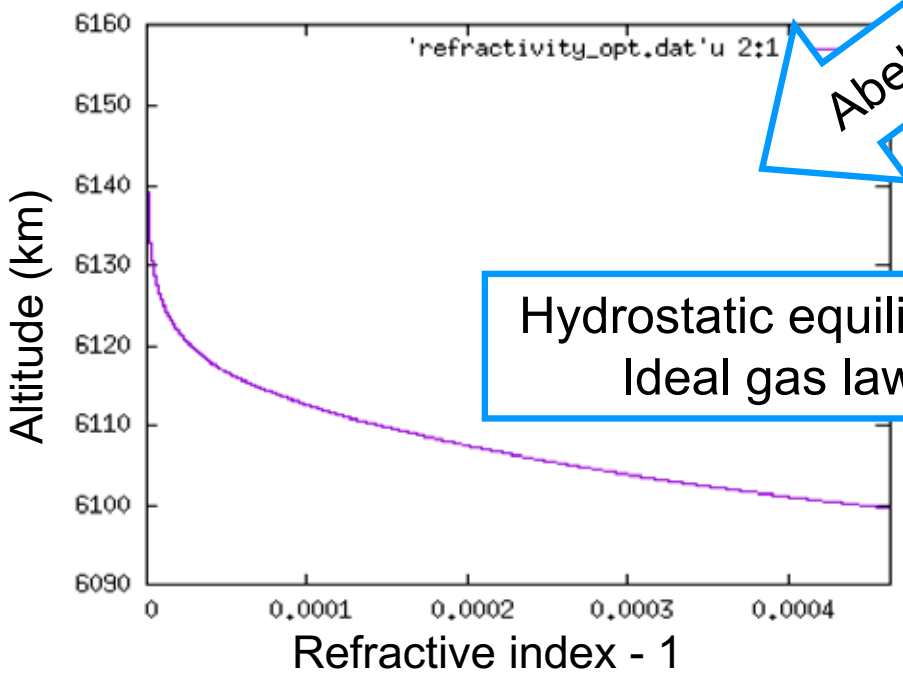

Hydrostatic equilibrium
Ideal gas law

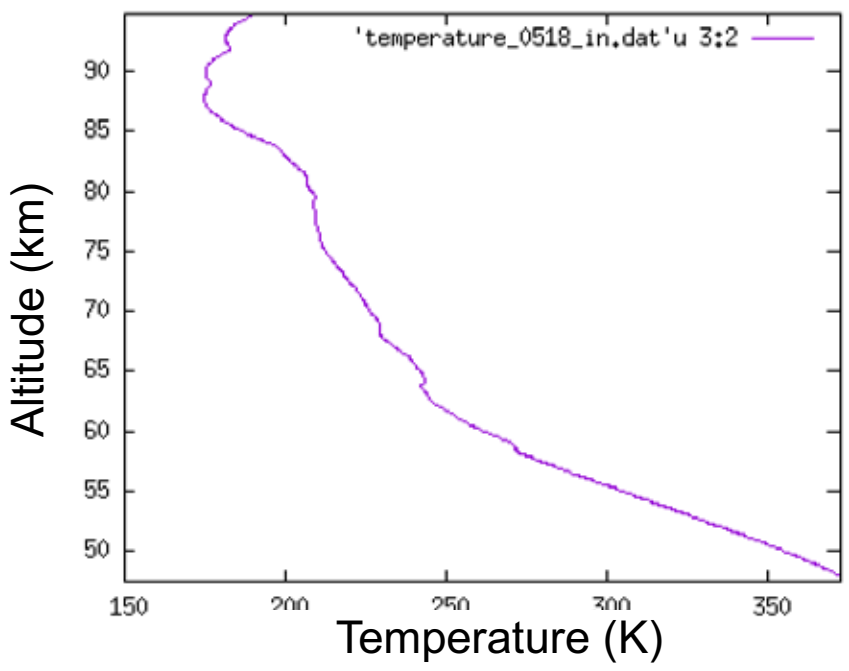

Temperature profiles of the Venus atmosphere obtained by Akatsuki radio occultation

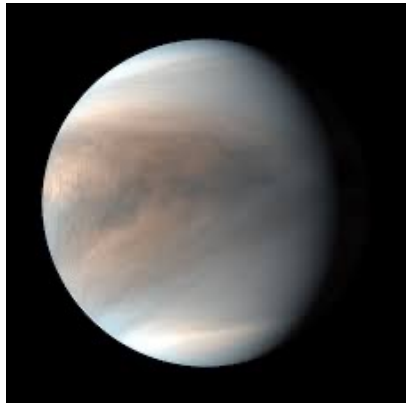

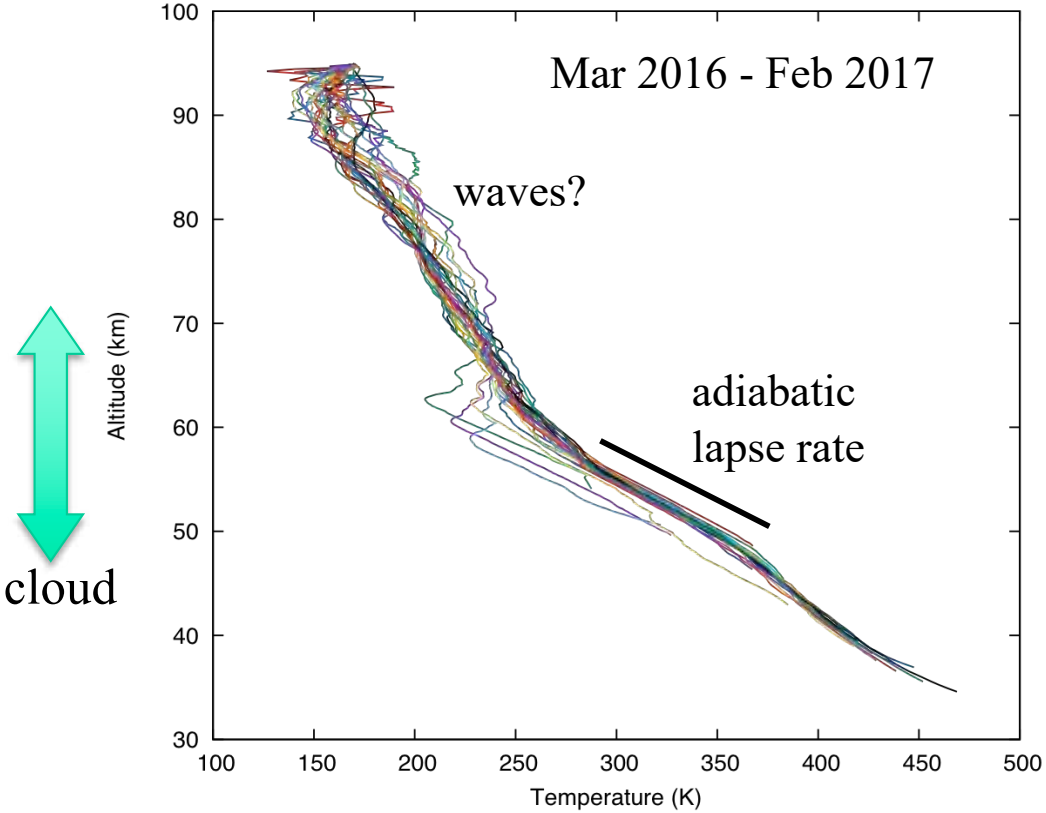

Imamura et al. 2017

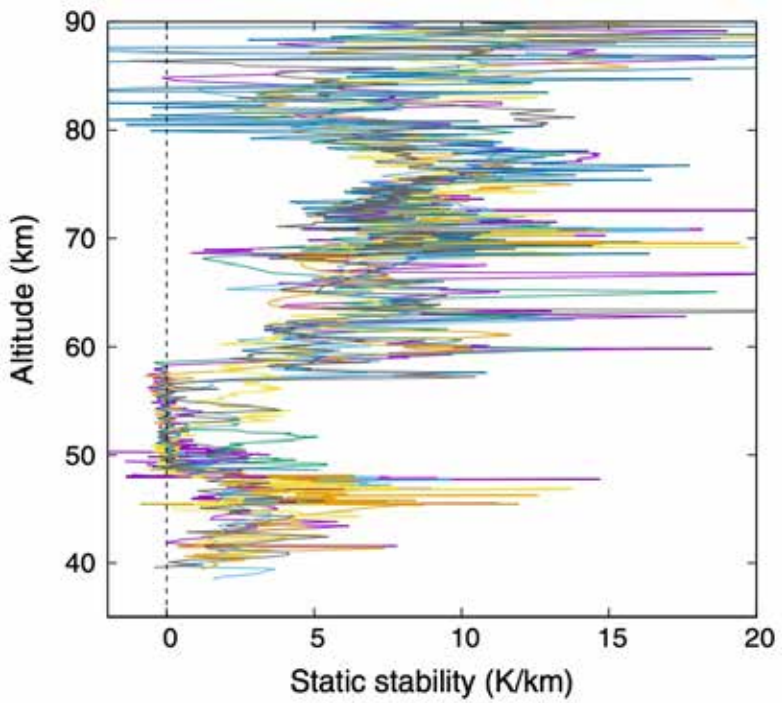

static stability: $S = \frac{dT}{dz} - \frac{g}{c_p}$

T : temperature
z : altitude
g : gravitational acceleration
c_p : specific heat for constant pressure

Radio occultation of Martian atmosphere

Convective boundary layer on Mars (Hinson et al. 2008)

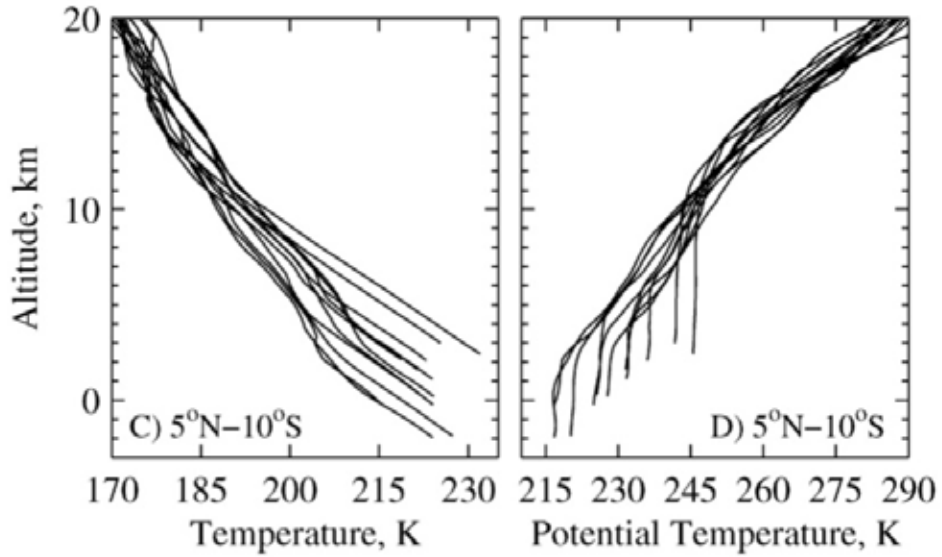

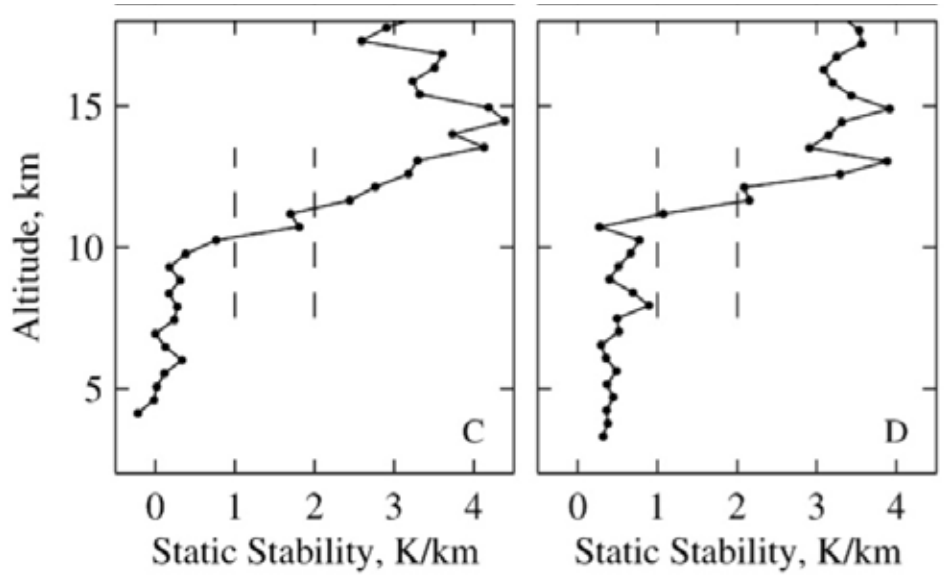

Examples of Venus' electron density profile from Akatsuki radio occultation

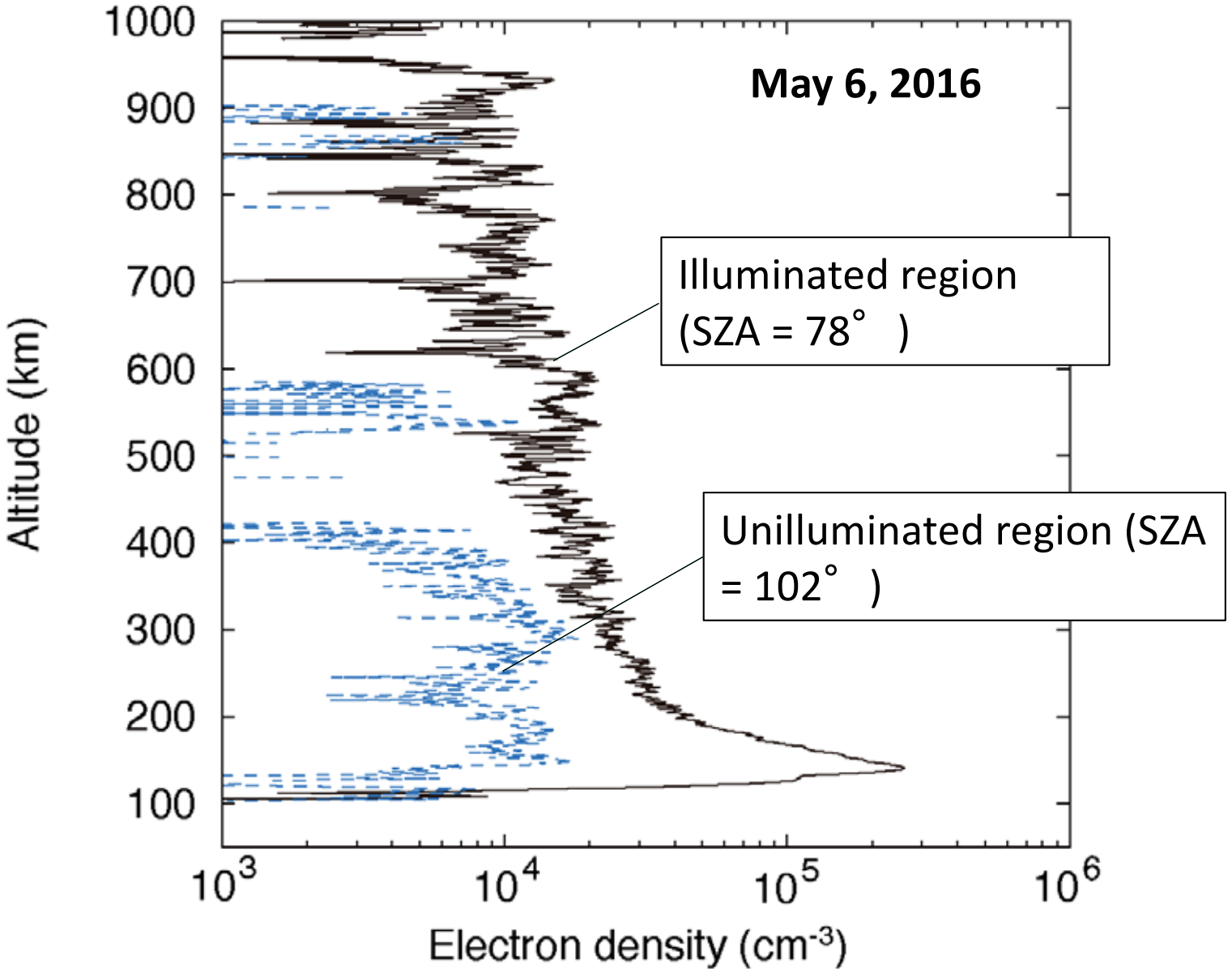

Dual-frequency method for plasma measurement

To remove the effect of the fluctuation of the transmitted signal's frequency and the neutral atmosphere's contribution, two frequencies generated from the common onboard oscillator are used. A linear combination of these phases can extract the plasma contribution.

plasma

oscillator noise + neutral atmosphere

$$\Delta\phi_S = -\frac{40.3}{c\,f_S}N_e + \alpha\, f_S \qquad \text{: Phase shift of S-band}$$

$$\Delta\phi_X = -\frac{40.3}{c\,f_X}N_e + \alpha\, f_X \qquad \text{: Phase shift of X-band}$$

$$\delta\phi = \Delta\phi_S - \frac{f_S}{f_X}\Delta\phi_X = -\frac{40.3}{c} f_S\left(\frac{1}{f_S^2} - \frac{1}{f_X^2}\right)\cdot N_e \qquad \text{: Differential phase}$$

N_e : Column electron density
f_S : S-band frequency
f_X : X-band frequency

Dual-frequency radio occultation of lunar photoelectron layer with SELENE

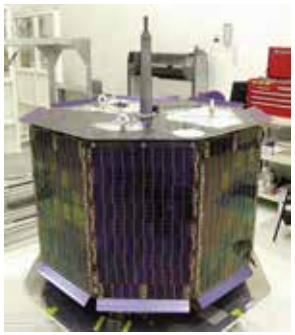

Vstar subsatellite

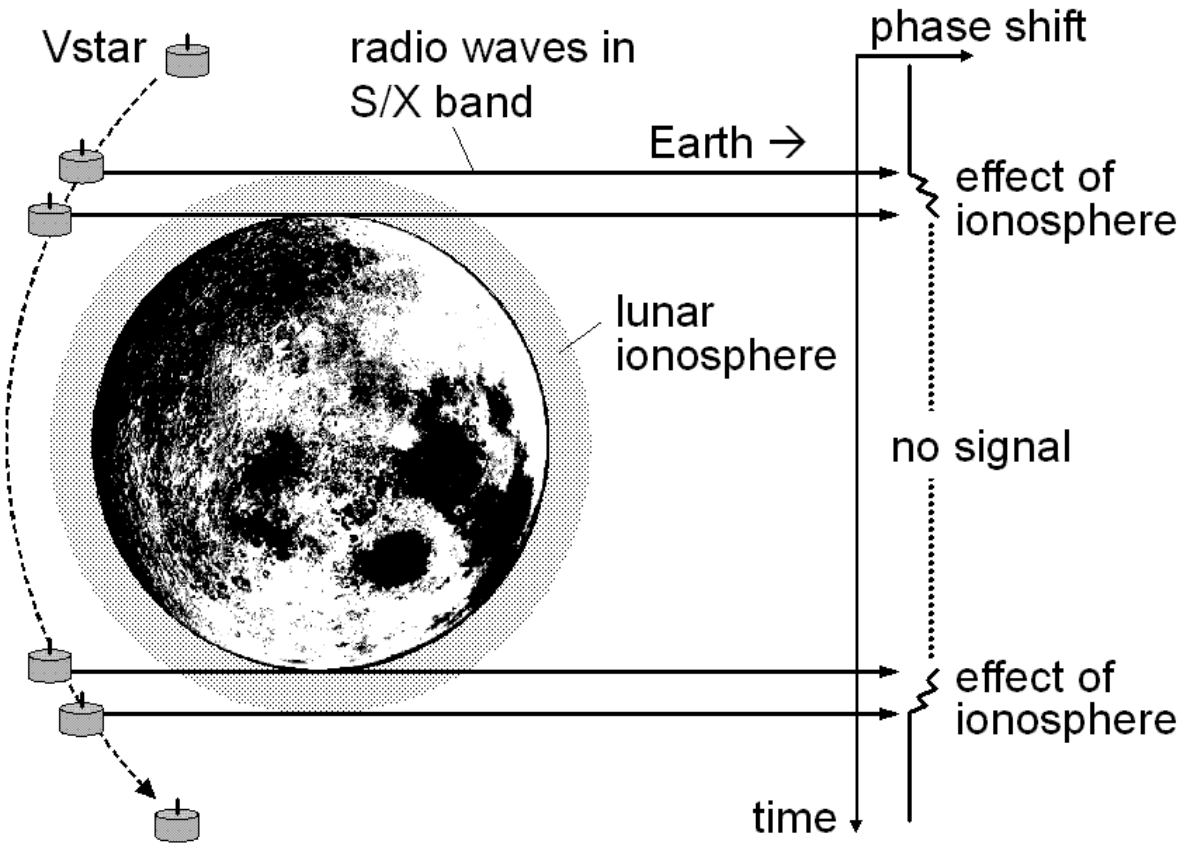

Usuda Deep Space Center, Japan

Example from lunar plasma layer measurement in SELENE mission

Phase in S-band (ϕ_S) and X-band (ϕ_X)

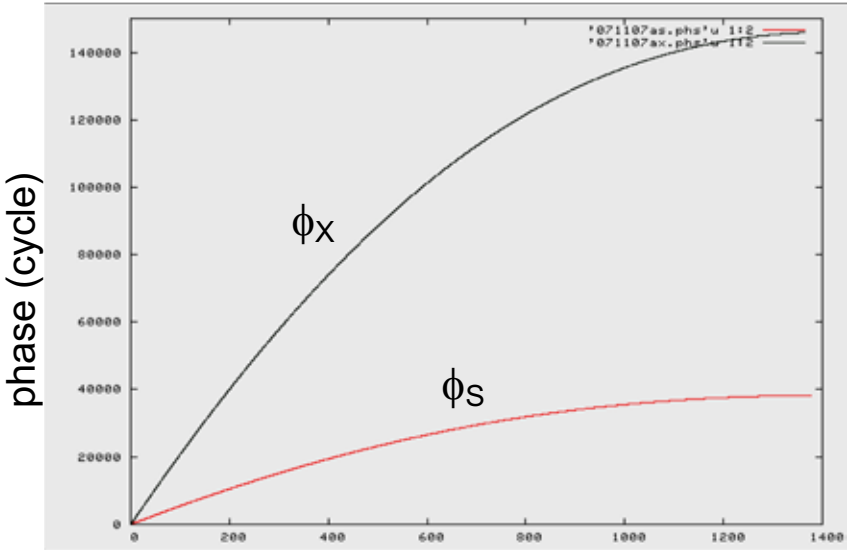

Differential phase $\phi_{diff} = \phi_S - f_s/f_x \phi_X$

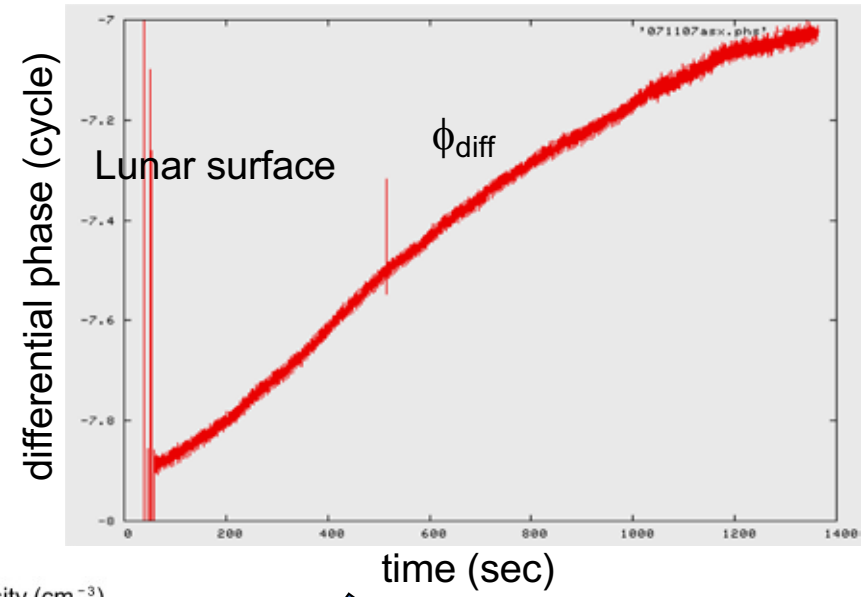

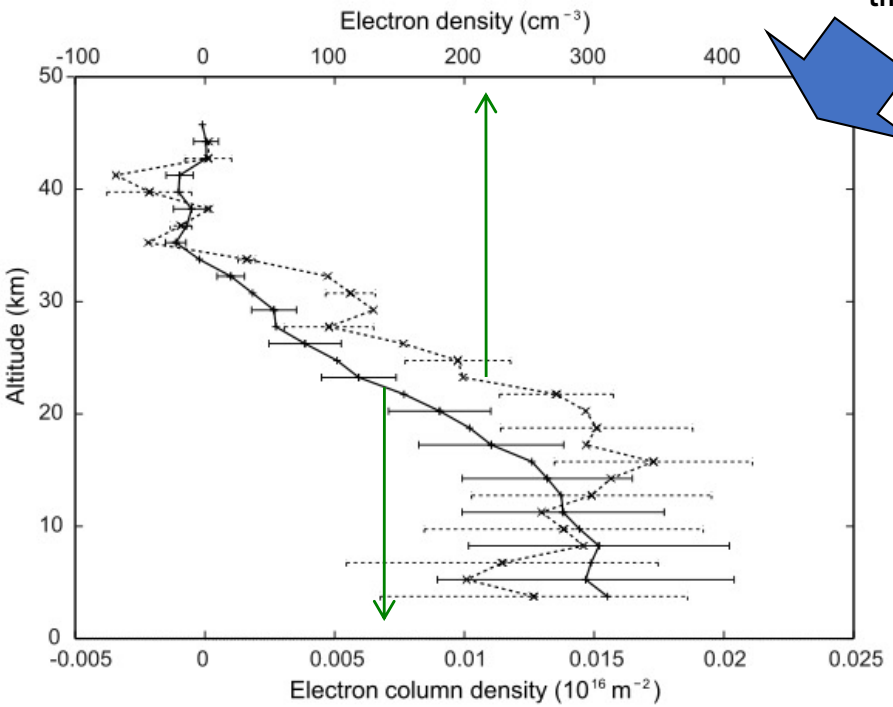

Imamura et al. (2012)

limitation of vertical resolution

$$F_n = \sqrt{\frac{n\lambda d_1 d_2}{d_1 + d_2}}, \quad d_1, d_2 \gg n\lambda,$$[3]

where

F_n is the nth Fresnel zone radius,

d_1 is the distance of P from one end,

d_2 is the distance of P from the other end,

λ is the wavelength of the transmitted signal.

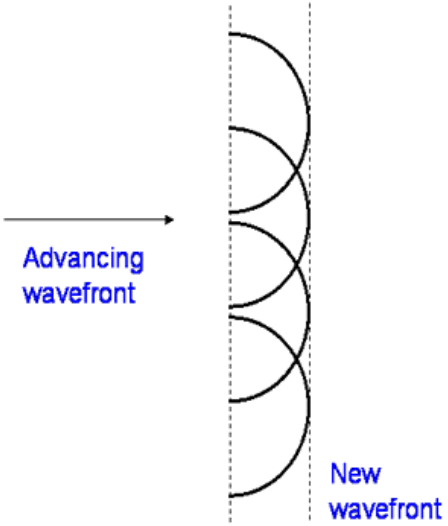

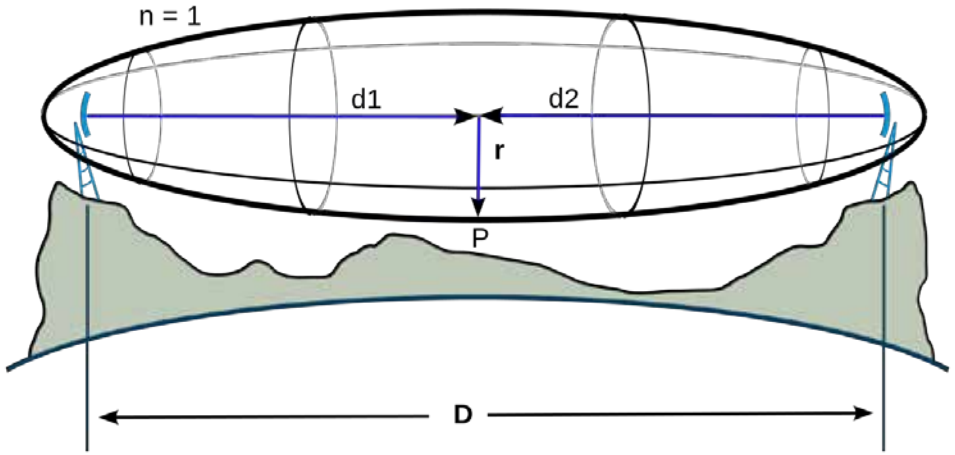

(Wikipedia)

n = 1 : First Fresnel zone. Outside this zone a destructive inference greatly reduces the contribution to the received signal.

F_1 is typically several hundred kilometers for interplanetary missions.

Multipath

An example of the signal spectrum time series

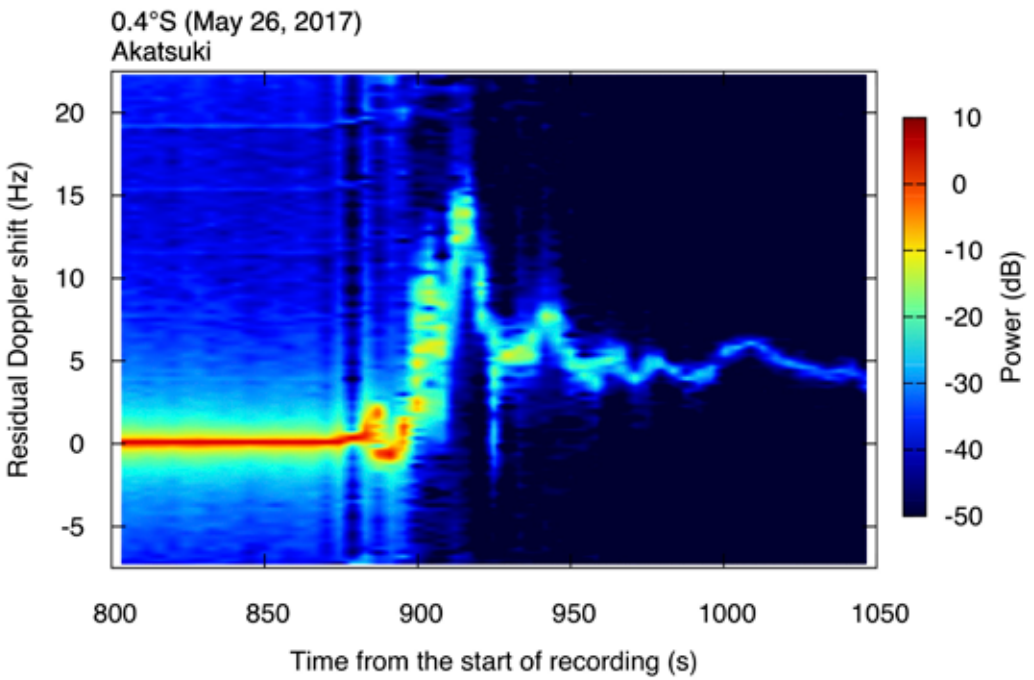

Schematic of multipath (Sokolovskiy, 2004)

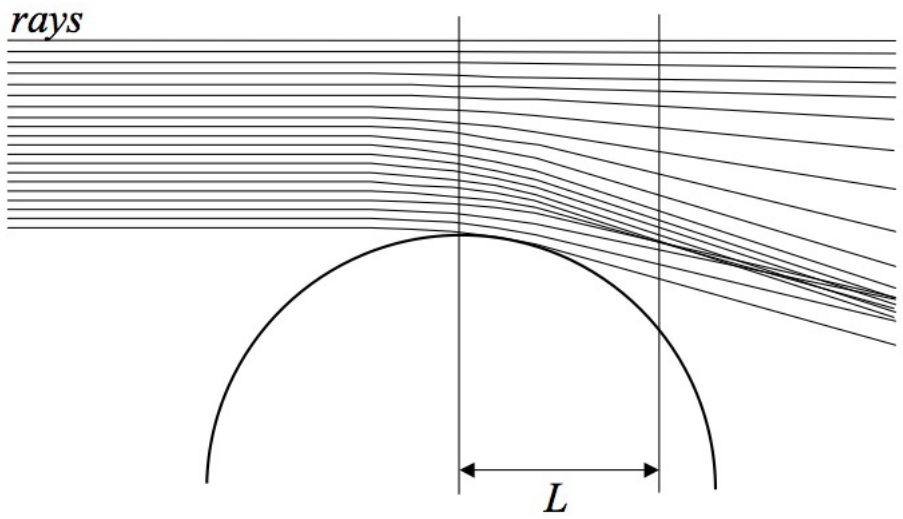

Radio holographic method can solve multipath problem (Imamura et al. 2018)

Radio holographic analysis

- One of the radio holographic methods, FSI ("Full Spectrum Inversion" Jensen et al. 2003) was applied to RS data.
- Spectral analysis is applied to the entire signal at once instead of applying it to successive short time blocks.

→High vertical resolution + Disentanglement of multipath

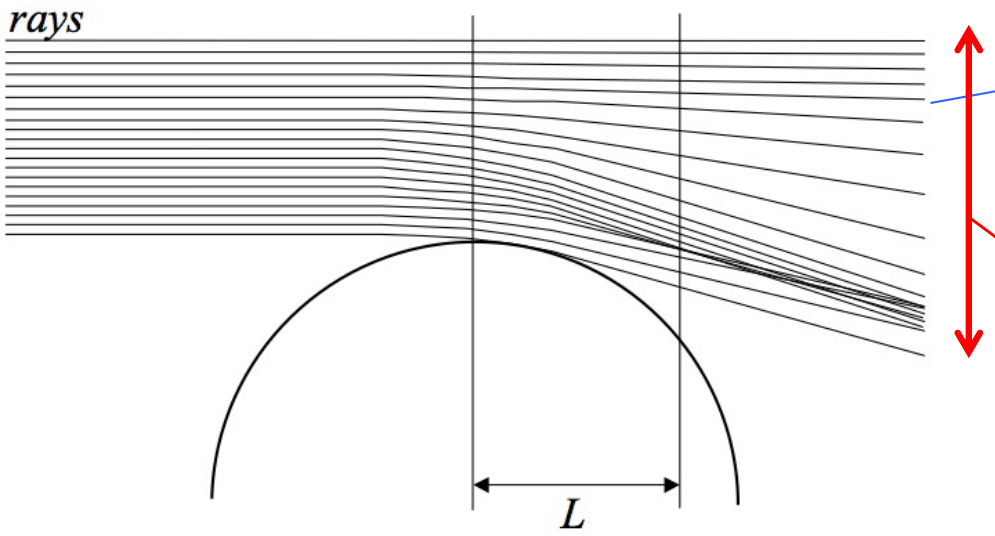

GO (geometrical optics) solves the instantaneous ray path at each time step

FSI solves the whole time series of the signal phase at once

Schematic of multipath (Sokolovskiy, 2004)

Radio occultation measurements of Pluto's neutral atmosphere with New Horizons

- Pluto has a tenuous atmosphere composed primarily of N_2.
- New Horizons spacecraft performed a radio occultation that sounded Pluto's atmosphere In 2015.
- Signals were transmitted by four ground antennas of the NASA Deep Space Network, and the spacecraft received the signals. The data streams were digitized, filtered, and stored on the spacecraft for later transmission to Earth.

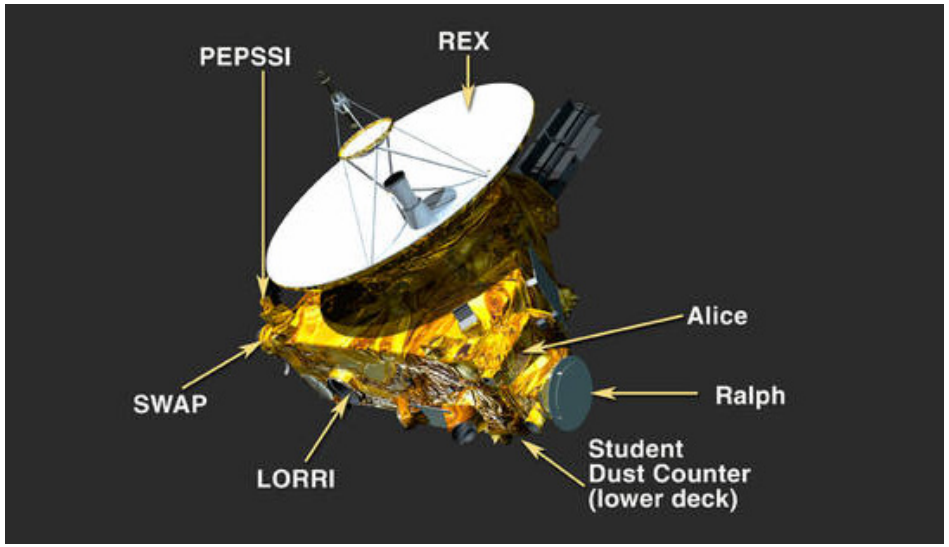

Hinson et al. (2017)

Removal of diffraction effects caused by the surface of Pluto

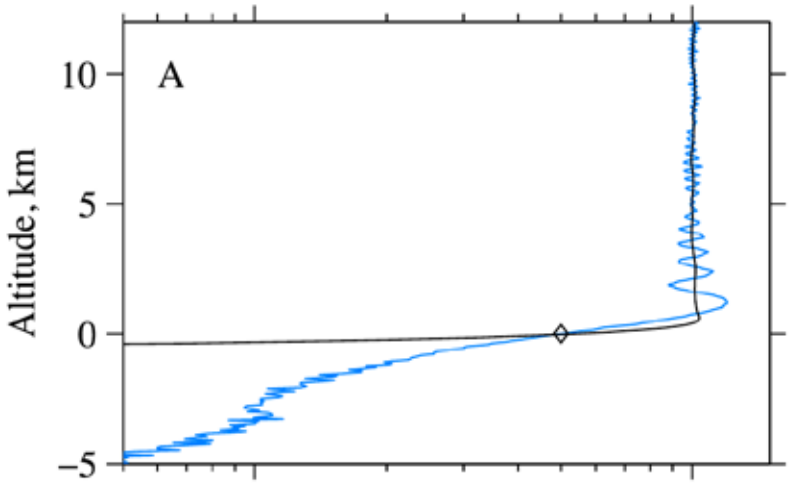

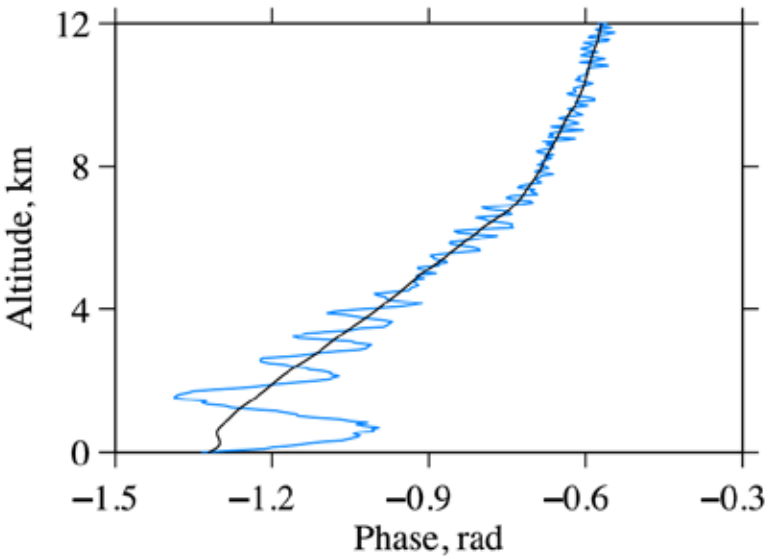

atmospheric profiles

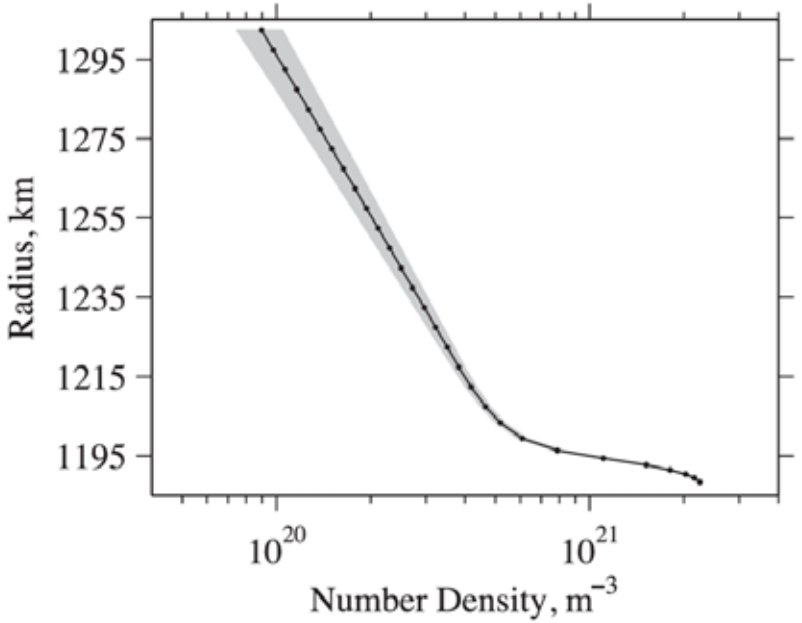

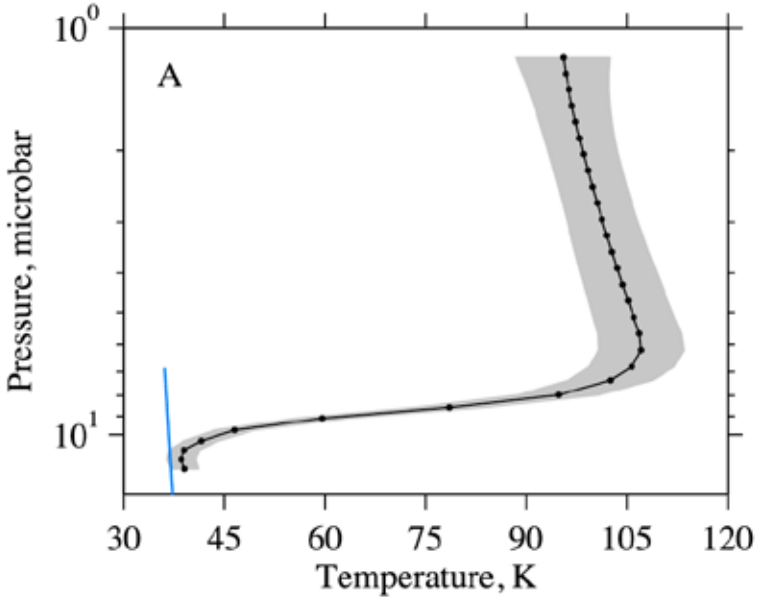

H_2SO_4 vapor in Venusian atmosphere deduced from radio wave absorption

Ingress occultation observed on May 6, 2016

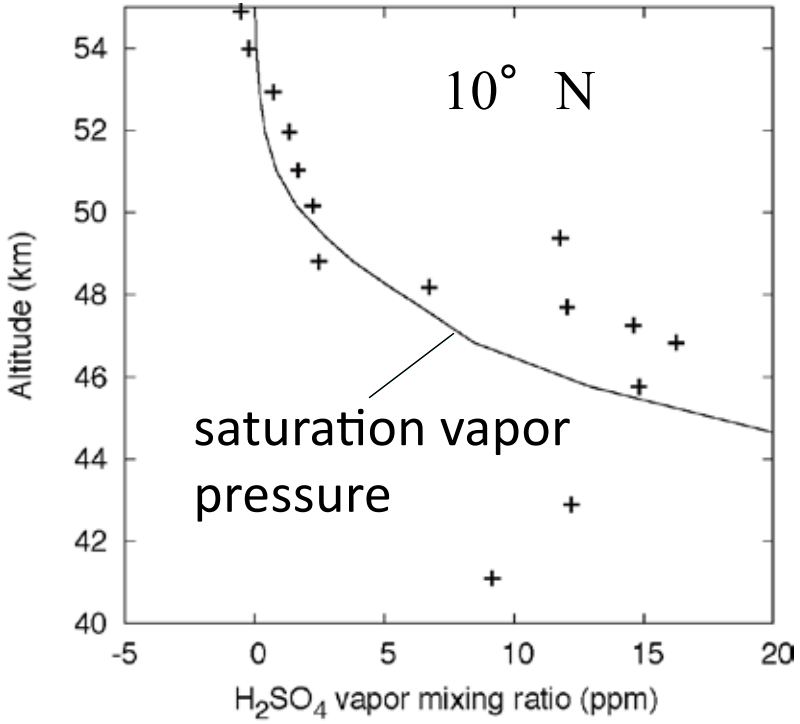

Imamura et al. (2017)

H_2SO_4 vapor measurement by Venus Express radio occultation

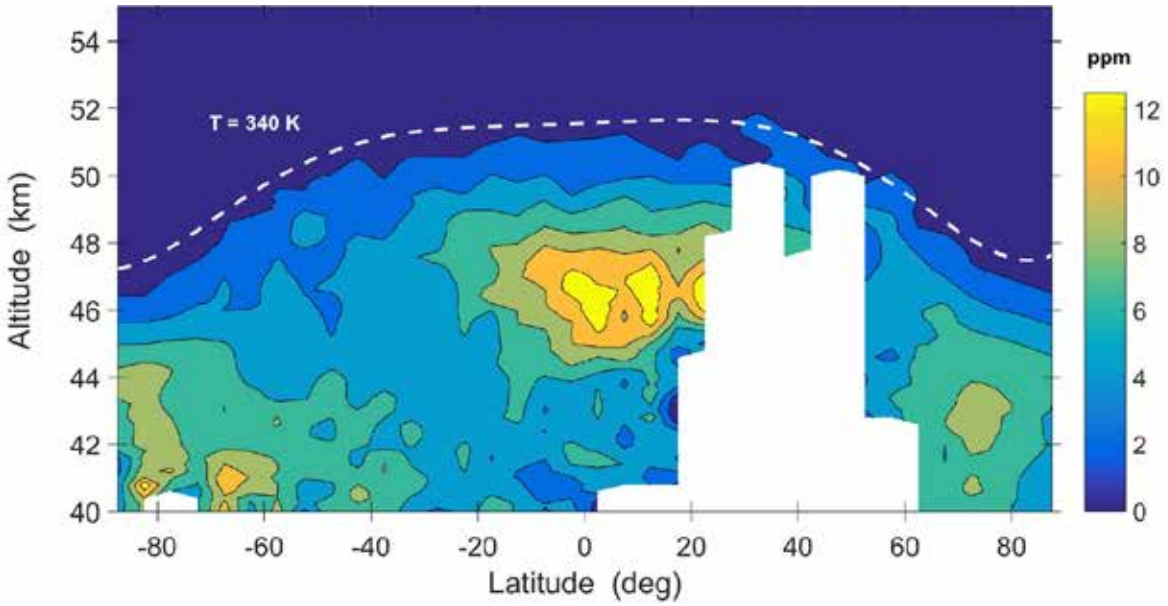

Oschlisniok et al. (2021)

GPS meteorology for Earth

UCAR/COSMIC homepage

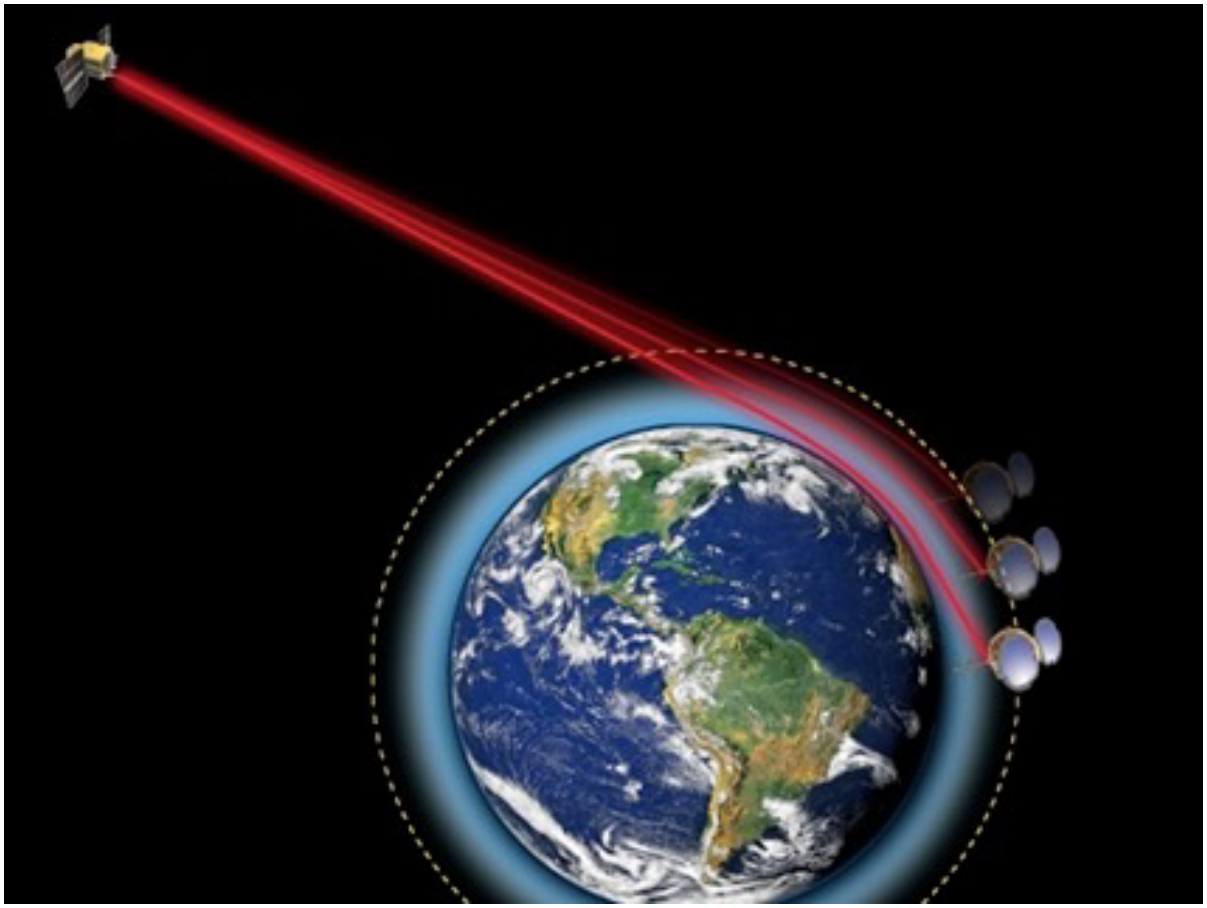

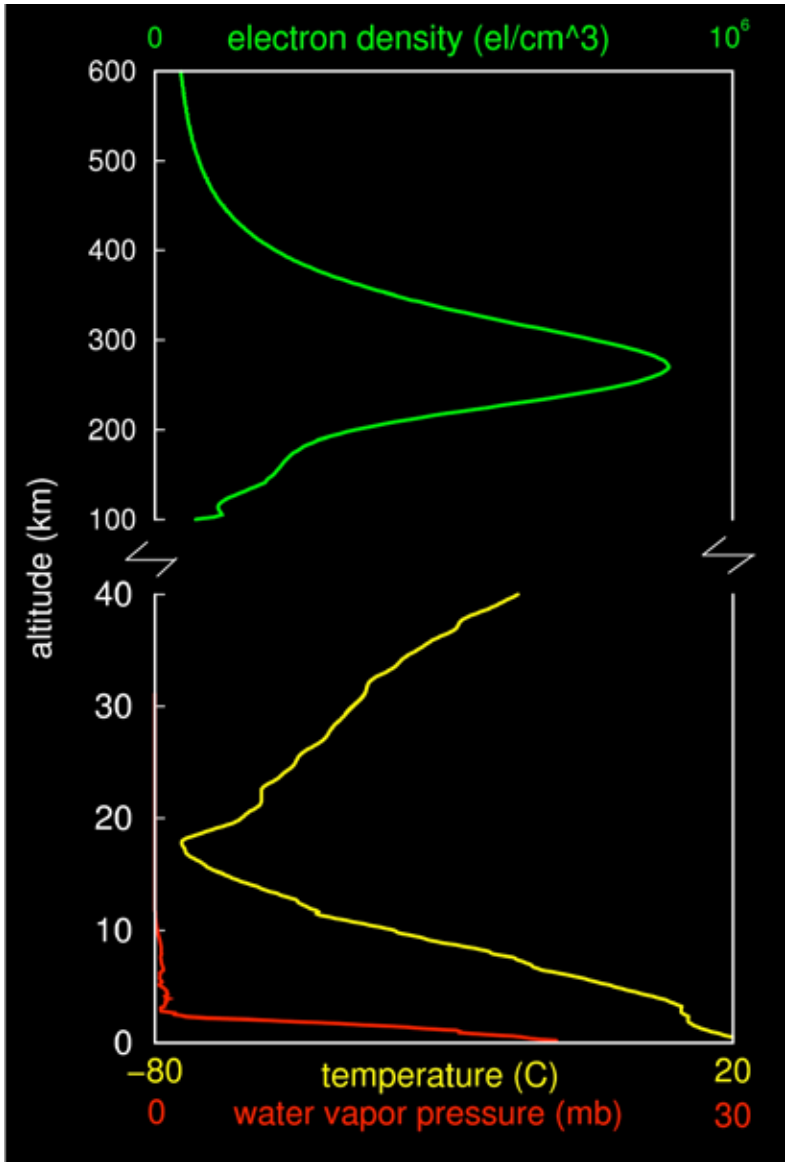

COSMIC : Constellation Observing System for Meteorology, Ionosphere, and Climate

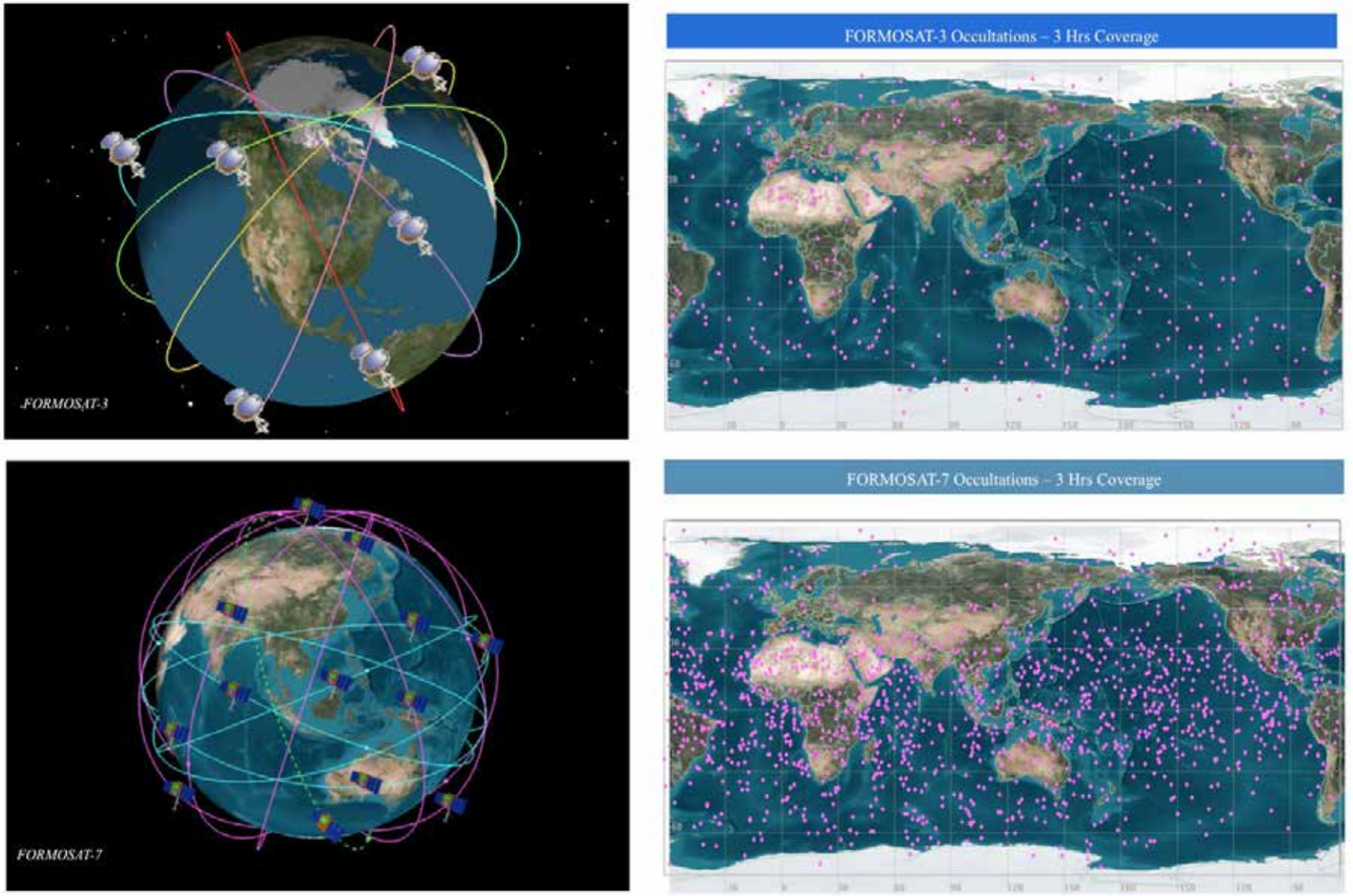

UCAR/COSMIC homepage

Fig. 1. Constellation design and estimated distribution of GPS RO soundings over a 3-h period from COSMIC/FORMOSAT-3 and COSMIC-2/FORMOSAT-7. The first tropical constellation of COSMIC-2 will be launched in 2016, and the second constellation will be launched in 2018. COSMIC-2 will provide an order of magnitude more GPS RO soundings over the tropics, which will have a significant impact on tropical cyclone prediction.

Radio occultation observation of the solar corona

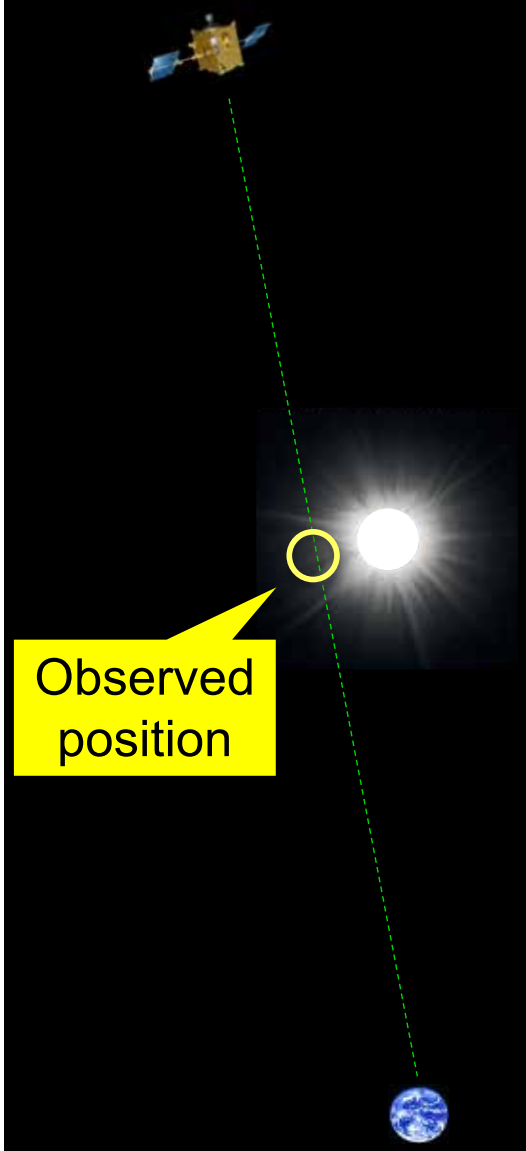

Radio occultation measurement using spacecraft signals is a powerful tool to probe the inner heliosphere.

Akatsuki's observation:

- Akatsuki was launched in 2010 and inserted into an orbit around Venus in 2015. During its solar conjunction, solar corona observation campaigns have been conducted.
- X-band (8.4 GHz) 1-way downlink using an ultra-stable oscillator (USO)
- Open-loop recording at the Usuda Deep Space Center, Japan

Intensity scintillation

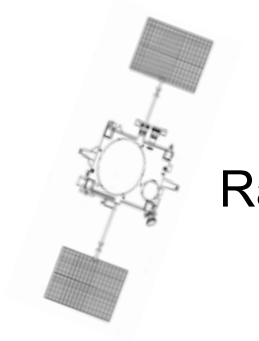

Radio wave

Movement of phase modulator relative to the ray path

Plane wave

Solar wind

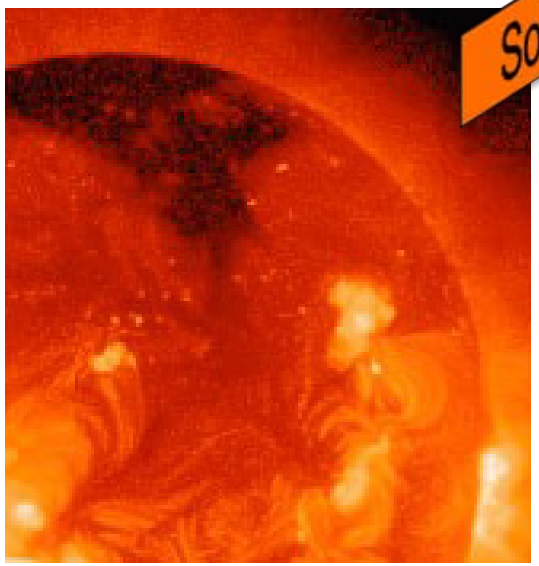

Phase modulating ‘screen’

Disturbed wave front

Diffraction pattern projected onto a screen (observer)

Fast wind and Slow wind

Observations in 2011
(Imamura et al. 2014, ApJ)

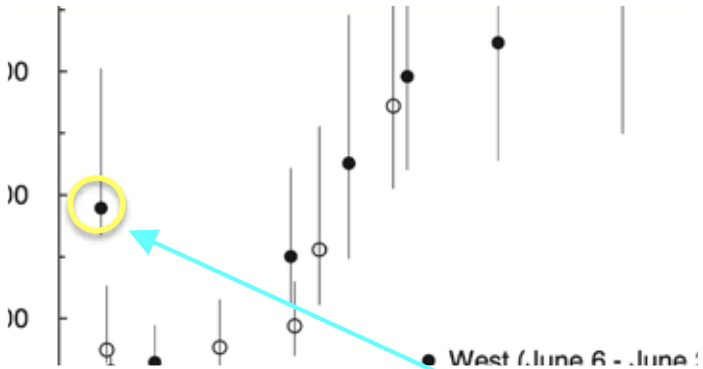

Observations in 2016
(Chiba et al., 2022)

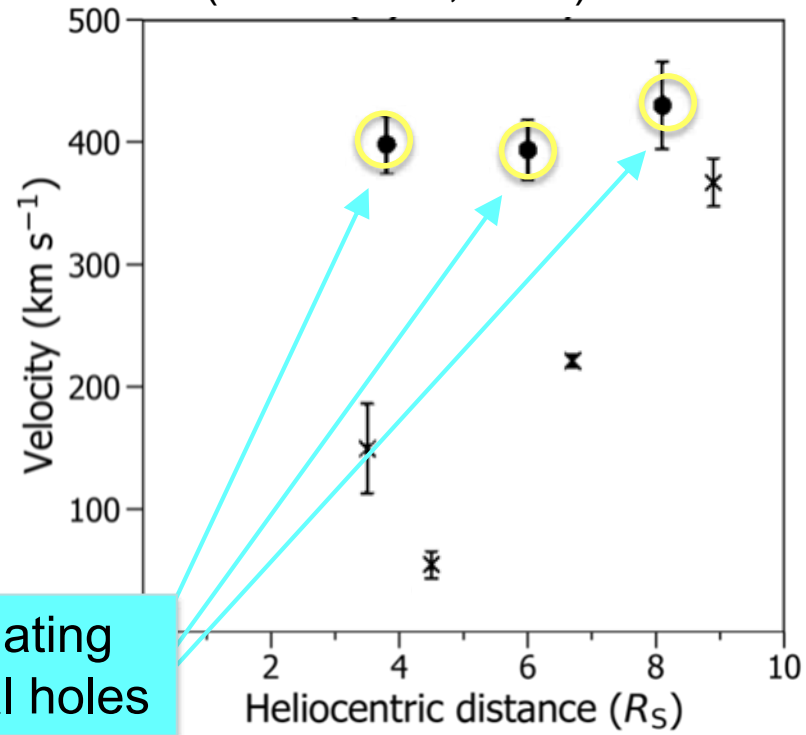

Flows originating
from coronal holes

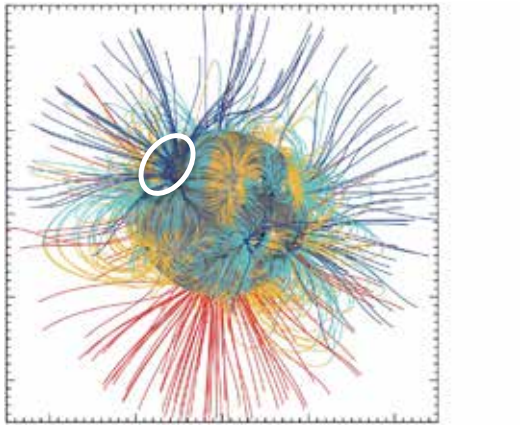

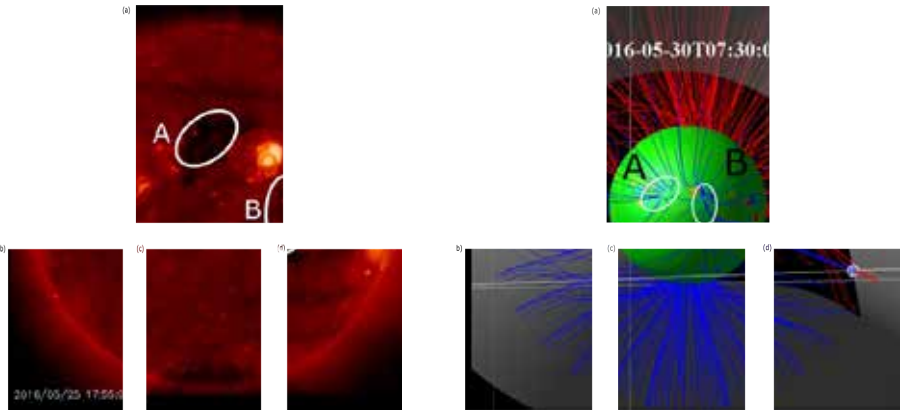

Phase/frequency fluctuation

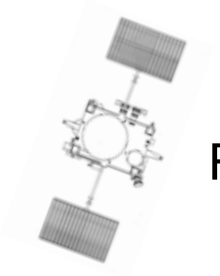

Radio wave

Movement relative to the ray path

Plane wave

Solar wind

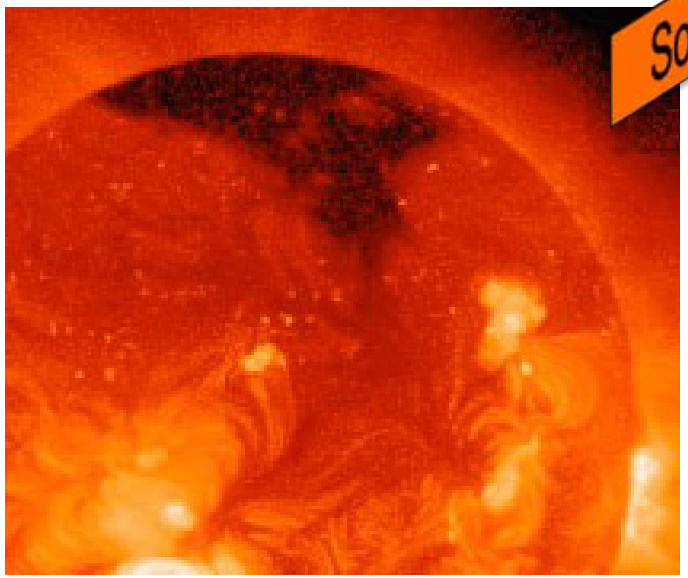

Density modulation

Phase modulation

ground antenna

Radial distribution of acoustic waves

Wavelet analysis
(Miyamoto et al. 2014, ApJ)

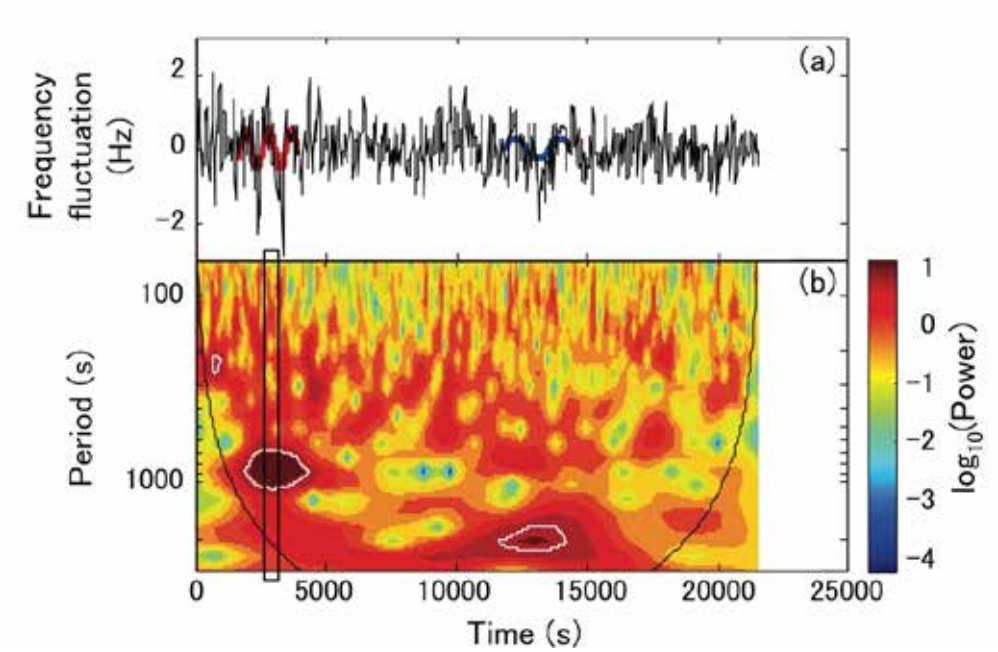

Local generation of large-amplitude acoustic waves ?

$\frac{n'}{n_0}$

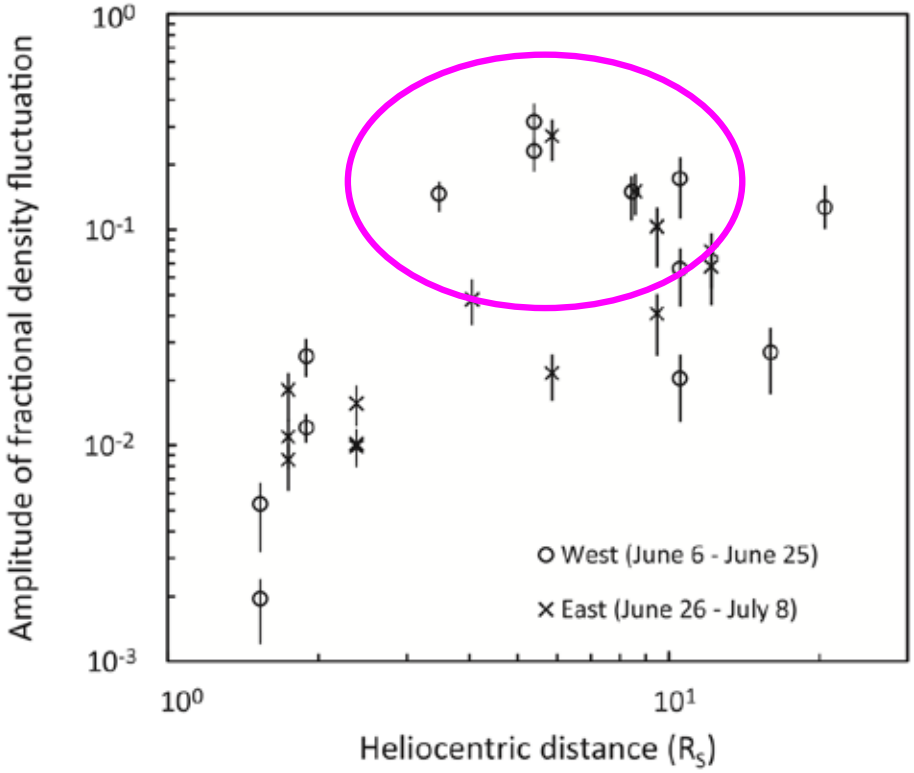

- The radial distribution suggests local generation of acoustic waves in the extended corona, probably through nonlinear dissipation of Alfvén waves that propagated from the photosphere.
- The dissipation of these waves will play key roles in coronal heating.

Radio occultation of rings

- Rings are composed of ice particles
- The radial profile of ring's optical thickness is obtained by the movement of the radio ray's intersection across the ring.
- Conducted by Voyager 1 and Cassini

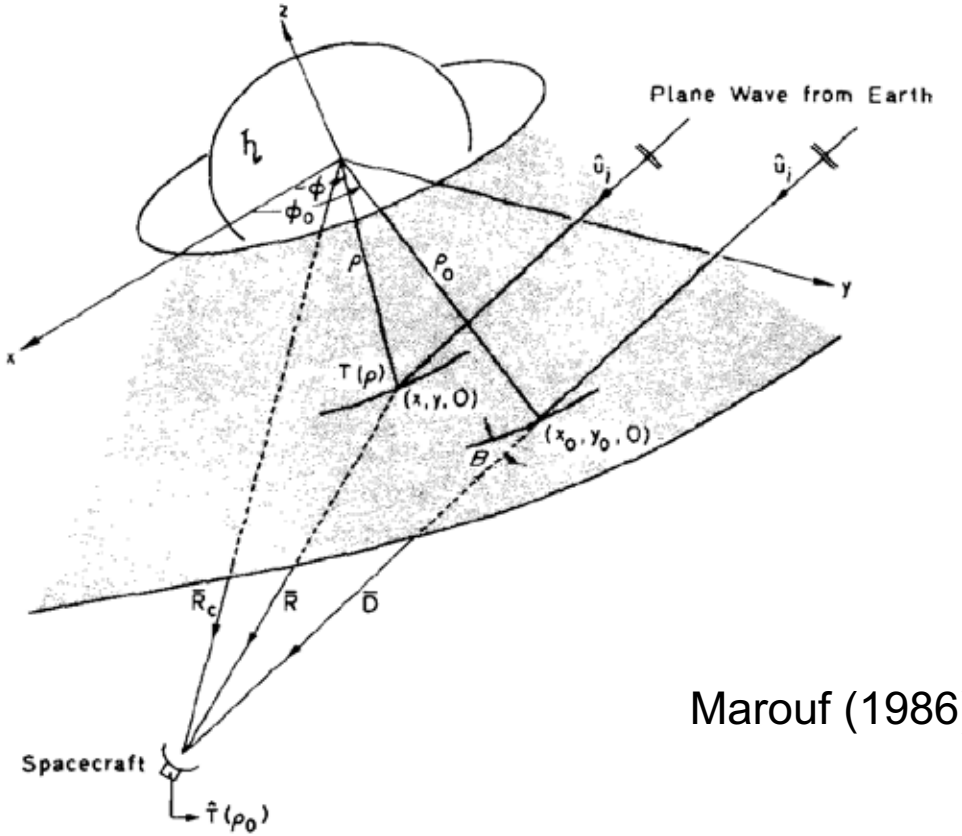

Marouf (1986)

Diffraction correction by inverse Fresnel transform

Diffraction by the edge of Encke gap

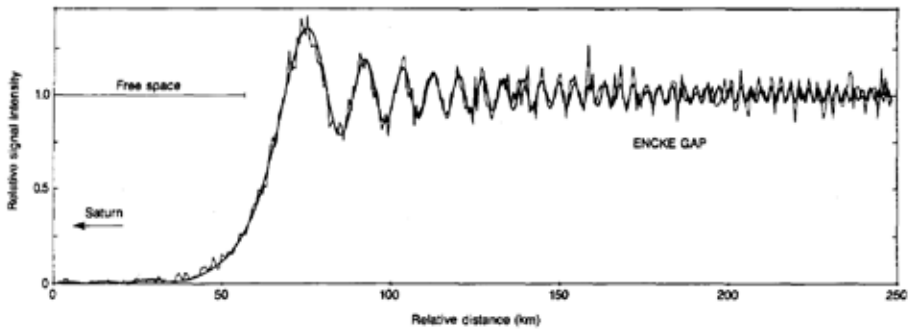

Tyler et al. (1987)

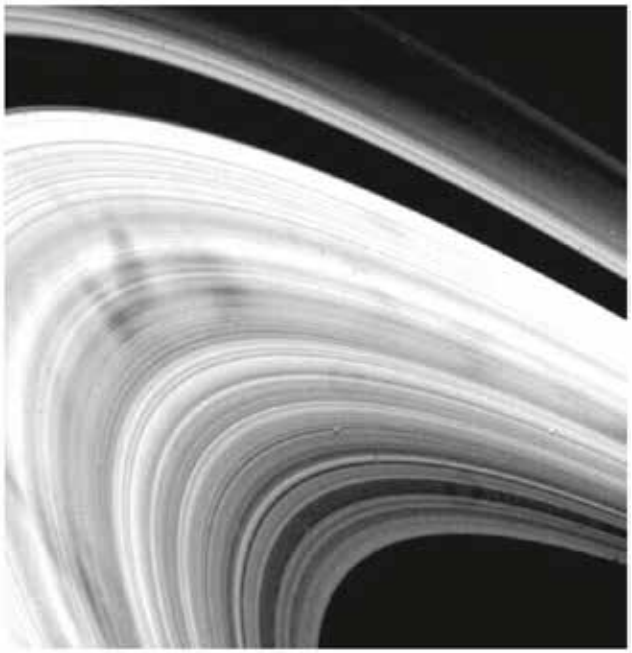

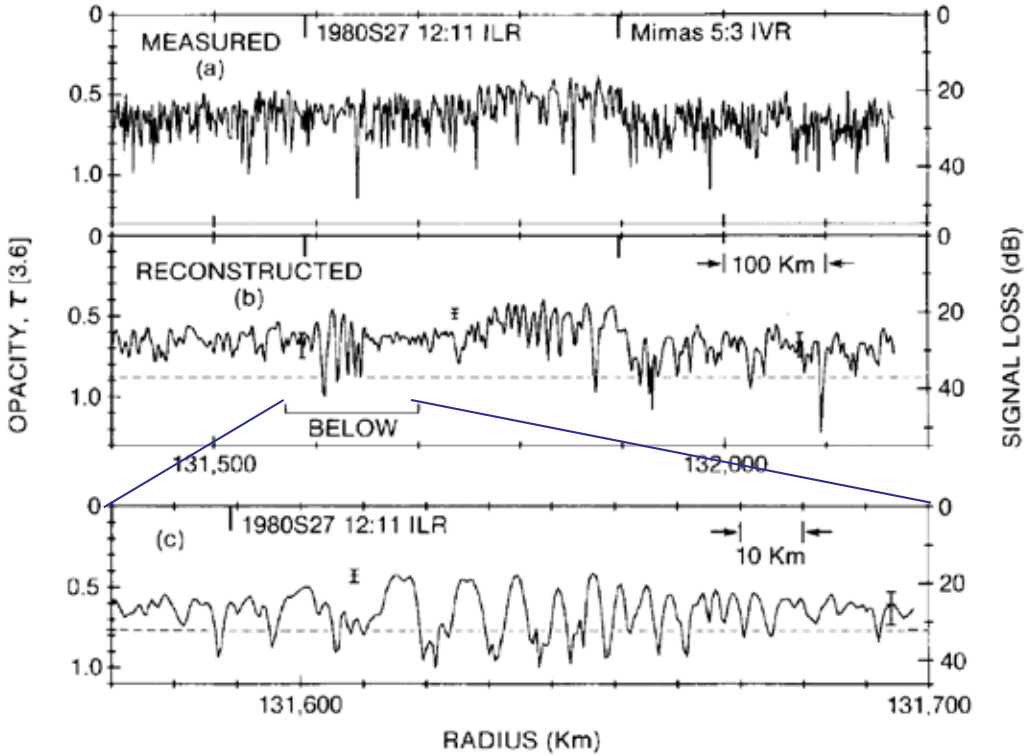

FIG. 15. (a) Measured and (b) reconstructed ($\Delta R_\phi \simeq 2.5$ km, $\lambda = 3.6$ cm) opacity profiles of a region 800 km wide in Ring A encompassing the 1980S27 12:11 density wave and the Mimas 5:3 bending wave. Theoretical locations of corresponding resonances are as indicated. Both waves are effectively masked in the initial diffraction-limited measurement. Note that the envelope of opacity minima of the bending wave is at a level noticeably smaller than the mean opacity level outside the wave region. (c) Many more oscillations of the density wave are revealed at 900 m effective resolution. Note that regions of opacity maxima are almost completely masked by noise at this resolution, however.

Marouf et al. (1986)

Doppler tracking of spacecraft to measure gravity anomaly

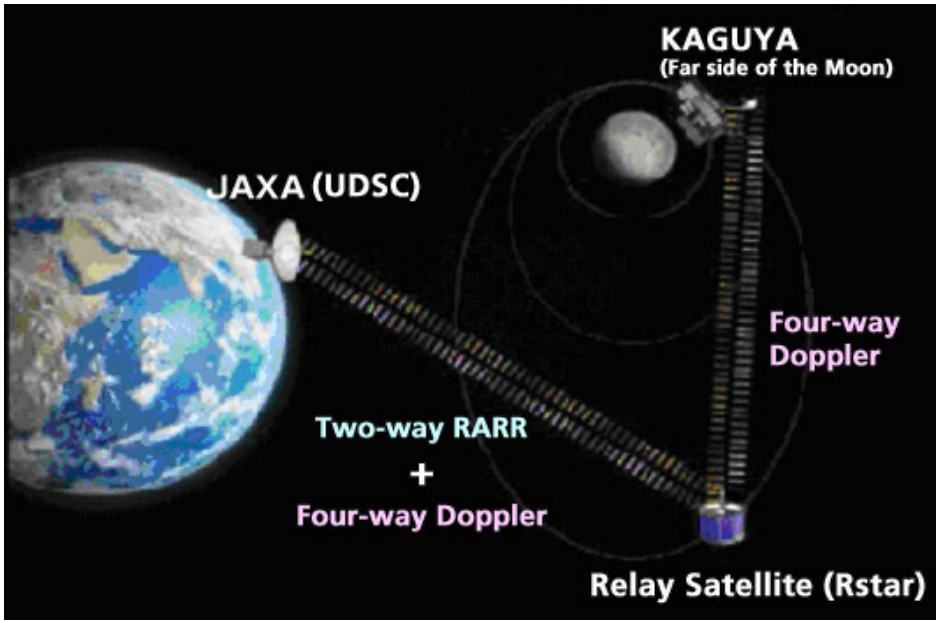

4way Doppler measurement using Relay satellite

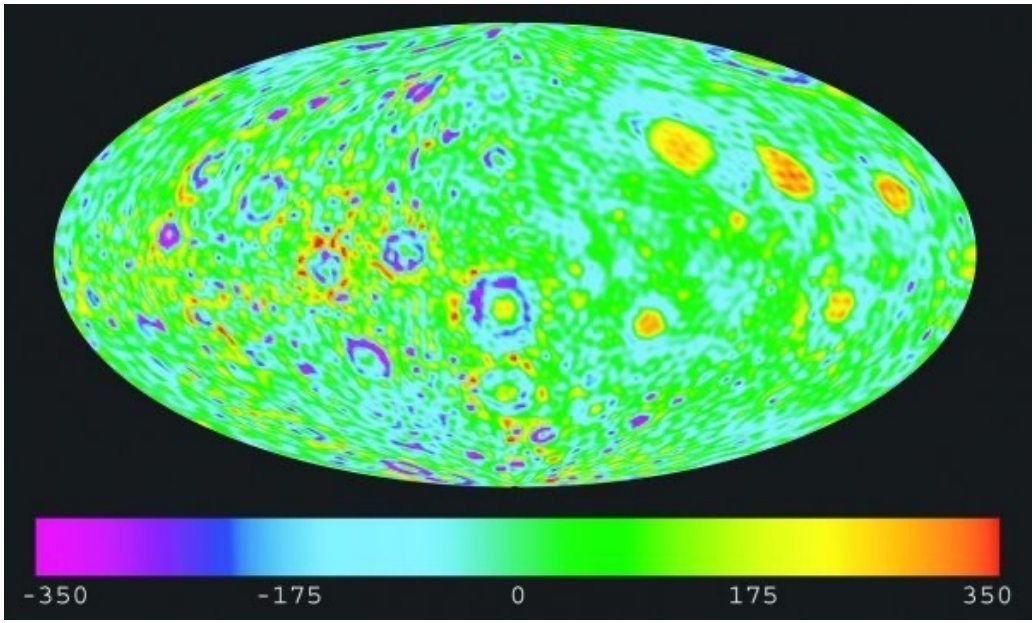

Gravity anomaly map of the Moon's surface obtained by JAXA's SELENE mission (in mGal = 10^{-5} m/s^2)

Doppler tracking of Juno spacecraft

- The spacecraft acts as a test particle falling in the gravity field of the planet. Jupiter's gravity is inferred from range-rate measurements between a ground antenna and the spacecraft during perijove passes.
- The ground station transmits two carrier signals, at 7,153 MHz (X band) and 34,315 MHz (Ka band). On board, an X-band transponder and a Ka-band frequency translator lock the incoming carrier signals and retransmit them back to the ground station at 8,404 MHz and 32,088 MHz, respectively. The range-rate (Doppler) observable is obtained by comparing the transmitted and received frequencies.

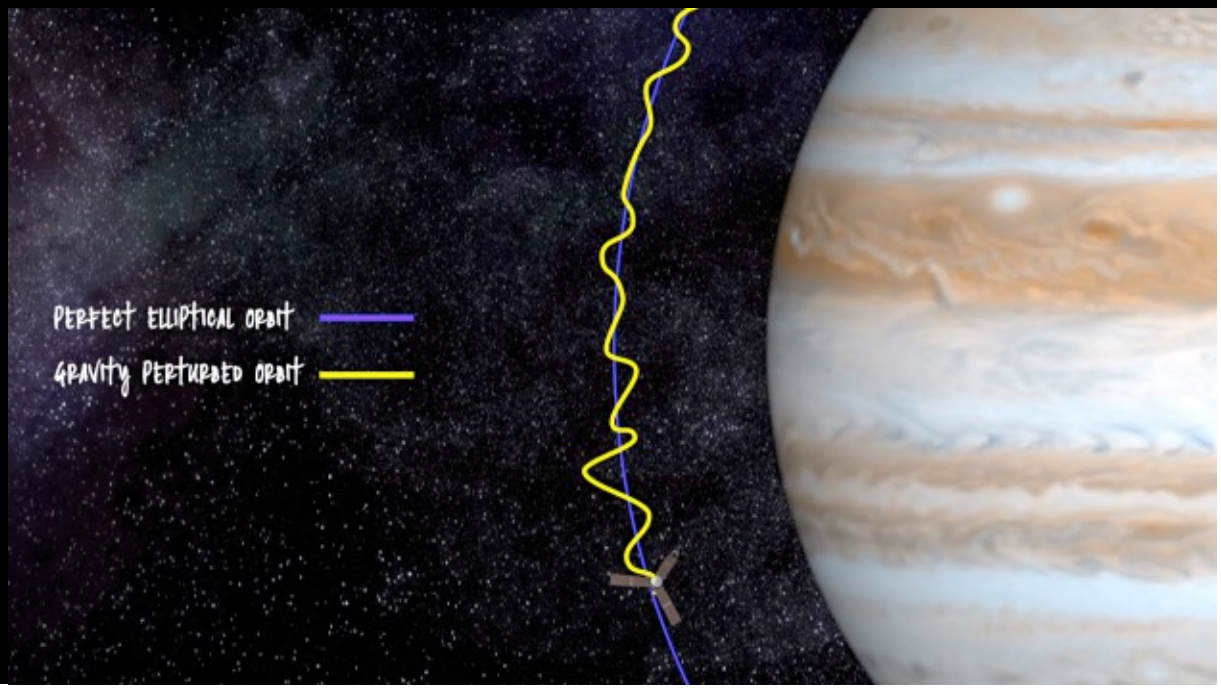

Less et al. (2018)

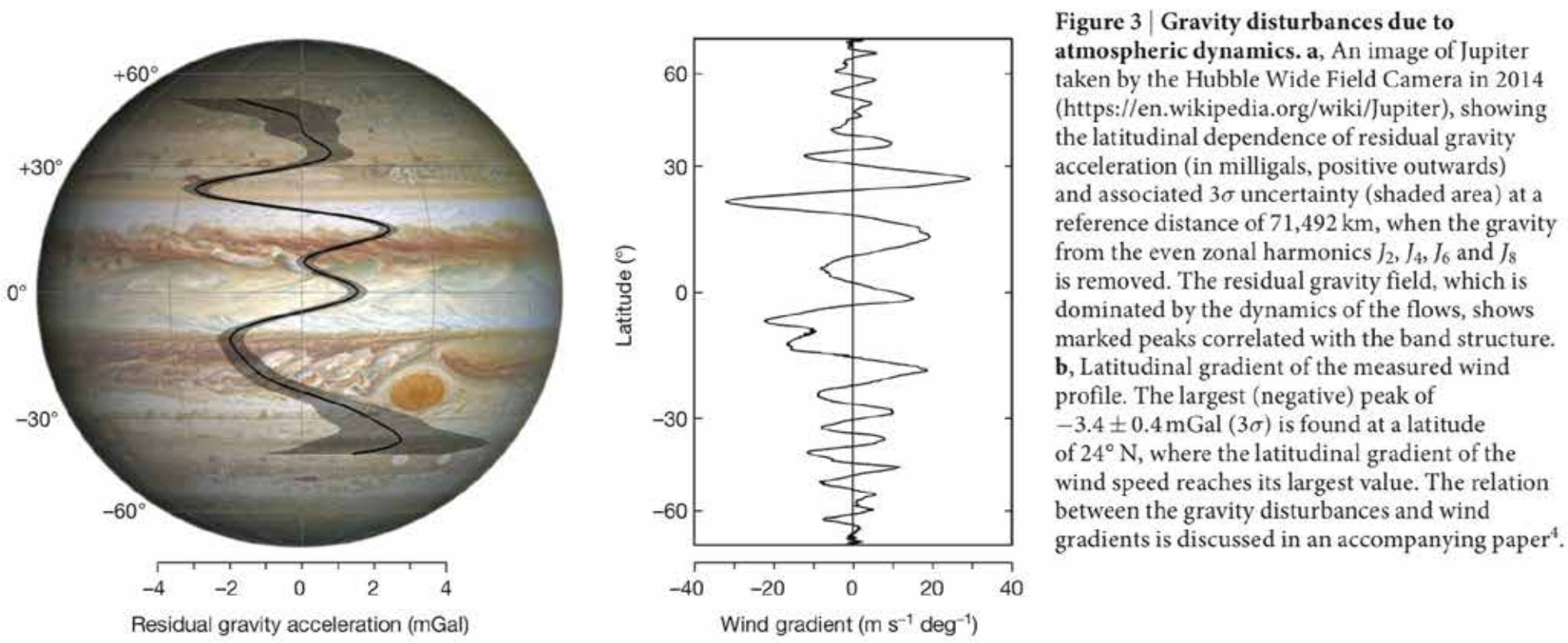

Figure 3 | Gravity disturbances due to atmospheric dynamics. a, An image of Jupiter taken by the Hubble Wide Field Camera in 2014 (https://en.wikipedia.org/wiki/Jupiter), showing the latitudinal dependence of residual gravity acceleration (in milligals, positive outwards) and associated 3σ uncertainty (shaded area) at a reference distance of 71,492 km, when the gravity from the even zonal harmonics J_2, J_4, J_6 and J_8 is removed. The residual gravity field, which is dominated by the dynamics of the flows, shows marked peaks correlated with the band structure. **b**, Latitudinal gradient of the measured wind profile. The largest (negative) peak of -3.4 ± 0.4 mGal (3σ) is found at a latitude of 24° N, where the latitudinal gradient of the wind speed reaches its largest value. The relation between the gravity disturbances and wind gradients is discussed in an accompanying paper[4].

"The observed jet streams, as they appear at the cloud level, extend down to depths of thousands of kilometres beneath the cloud level, probably to the region of magnetic dissipation at a depth of about 3,000 kilometres"

Microwave radiometer

JUNO/MWR

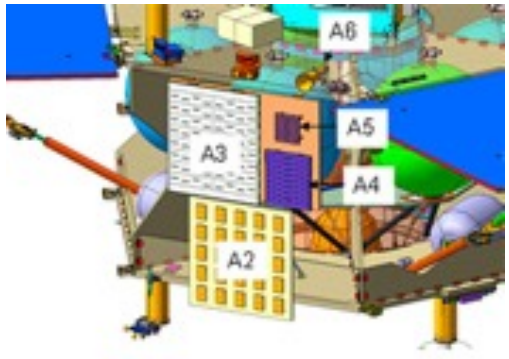

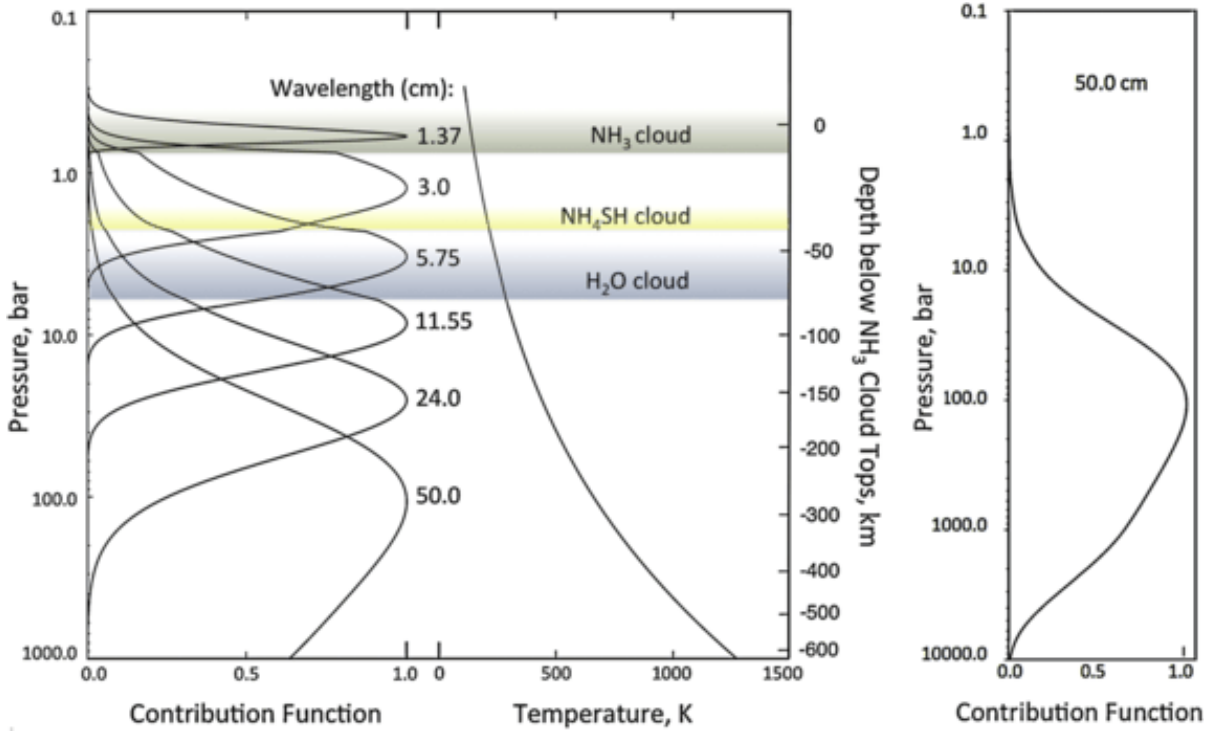

- Six antennas measure radio waves at frequencies 600 MHz, 1.2, 2.4, 4.8, 9.6 and 22 GHz
- Abundance of water and ammonia (NH_3) in the deep layers of the atmosphere up to 500–600 km deep
- The combination of different wavelengths and the emission angle should make it possible to obtain a temperature profile at various levels of the atmosphere.

Li et al. (2017)

NH_4 concentration (in ppm)

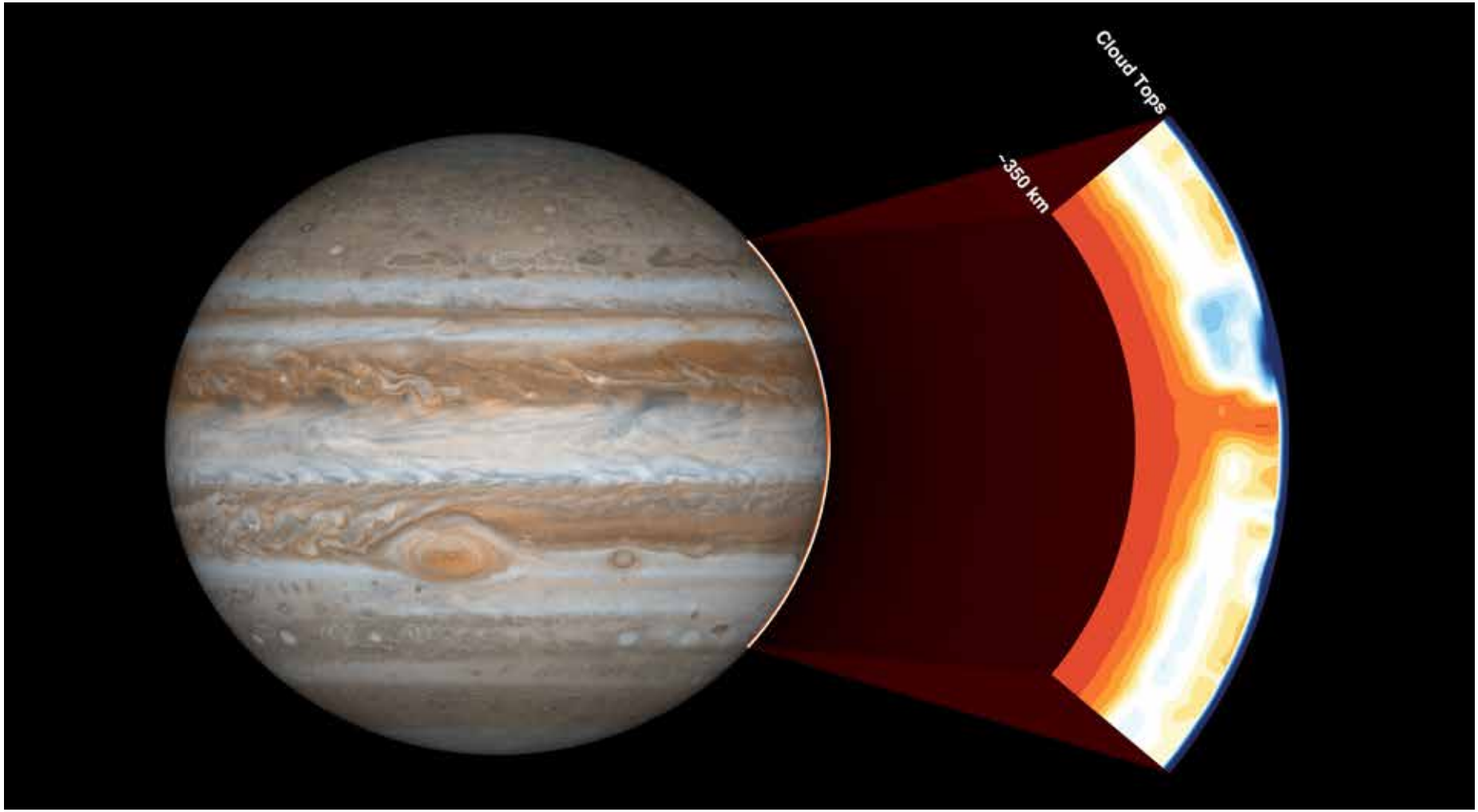

Figure 4. The colored contours show the ammonia concentration in parts per million inverted from nadir brightness temperatures during PJ1 flyby assuming that the deep water abundance is 0.06% (0.65 times solar). The deep ammonia abundance is 373 ppm, and the reference temperature is 132.1 K at 0.5 bar. The aspect ratio in the horizontal and vertical is exaggerated.

Microwave spectroscopy

ISS/SMILES to measure trace gases in Earth's stratosphere

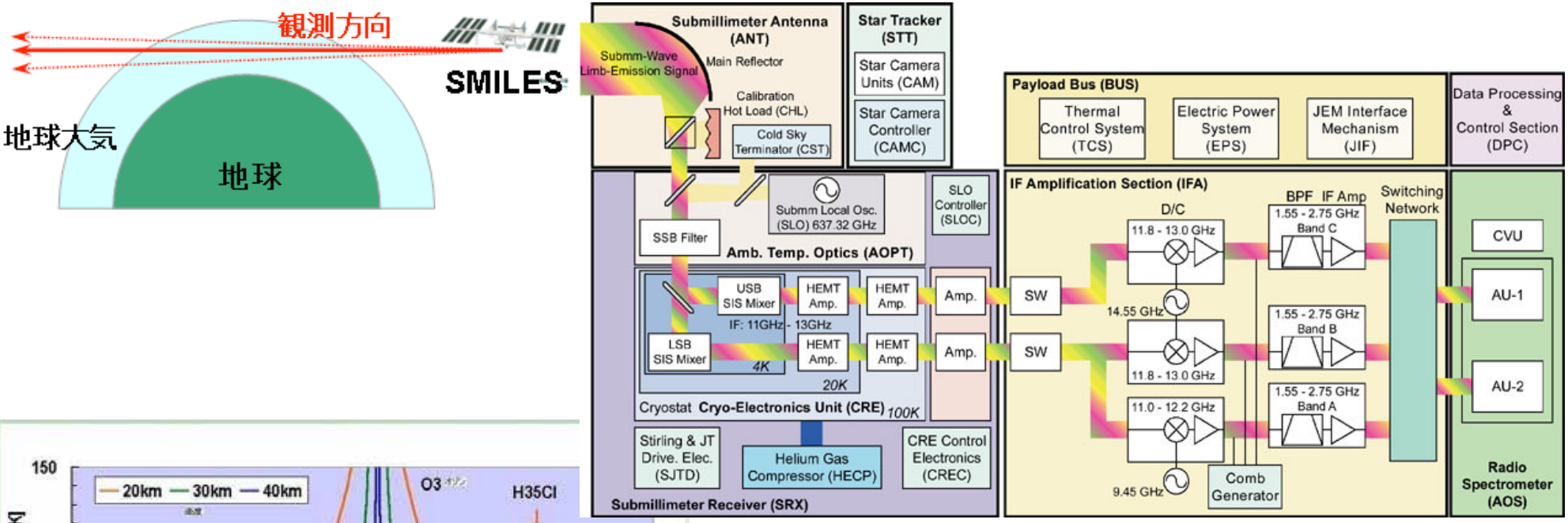

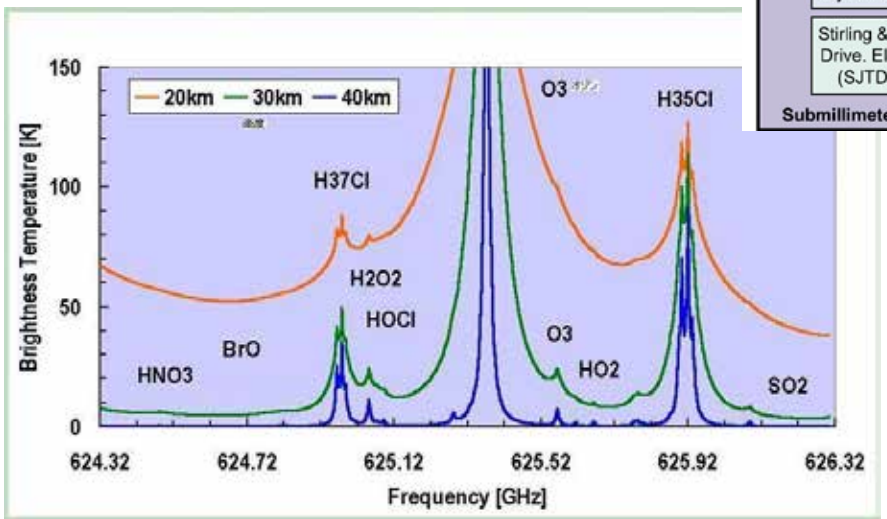

SMILES HP

An application of radio science technique

ISS/SMILES for Earth's stratosphere

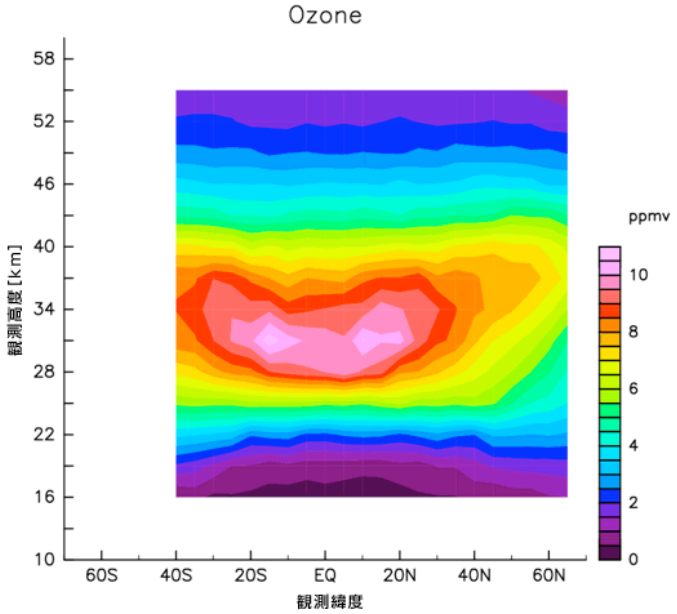

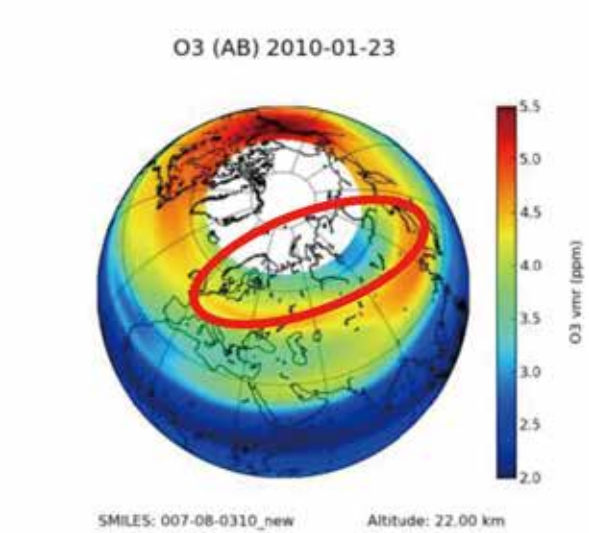

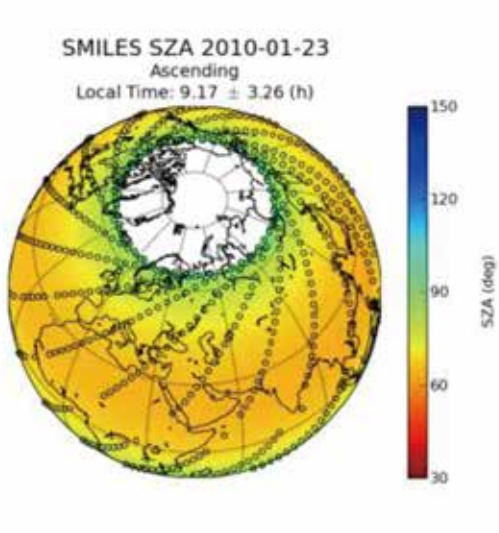

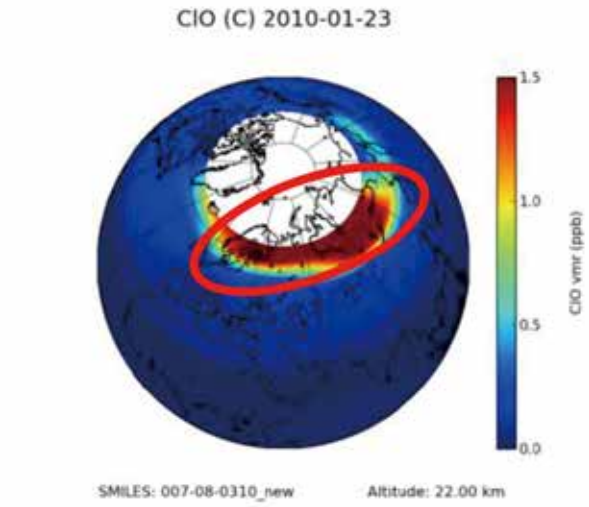

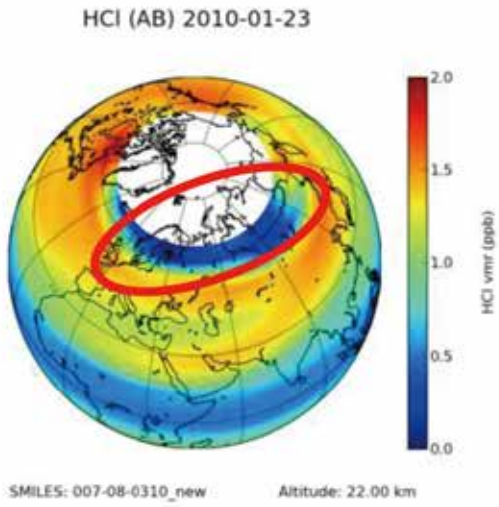

SMILES HP

JUICE(Jupiter Icy Moon Explorer)/ SWI(Submillimetre Wave Instrument)

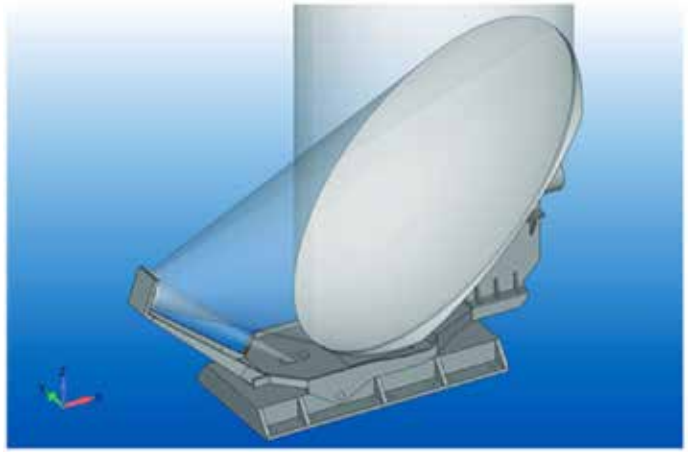

Kasai et al. (2014)

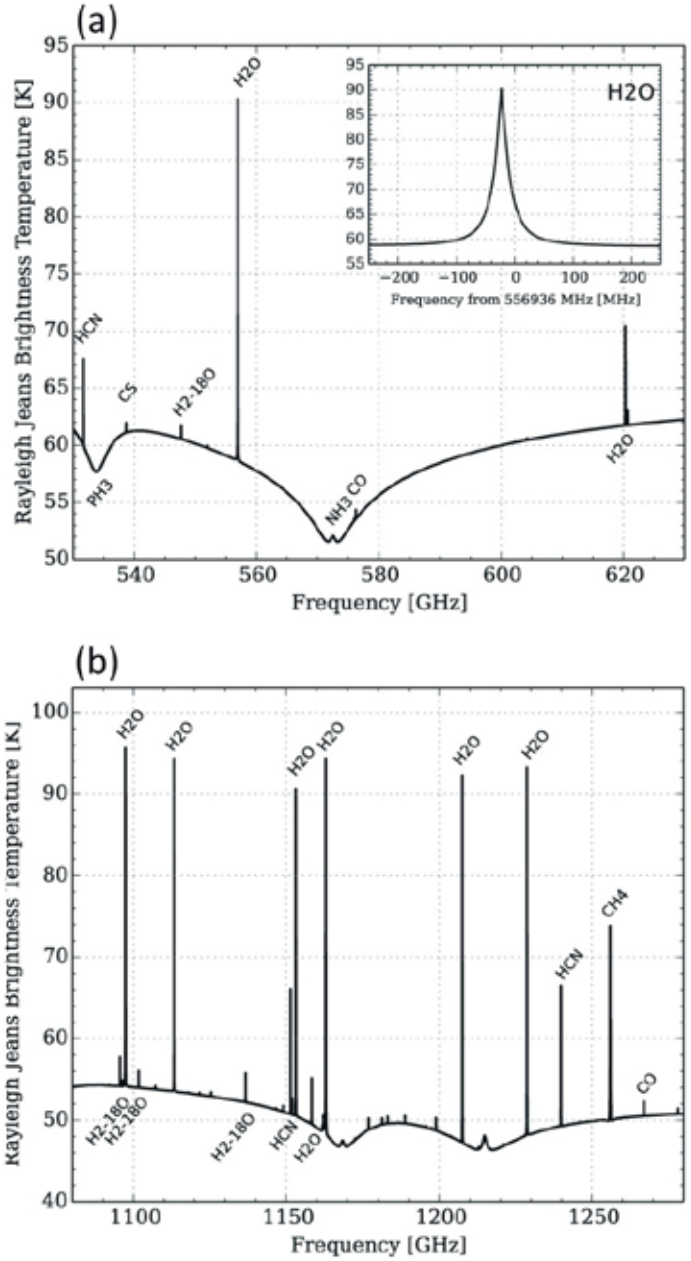

図1：SWIの観測周波数帯である(a)600 GHz帯および(b)1200 GHz帯における木星大気スペクトル(リム放射)のシミュレーション図．1000 hPaの接線高度を観測したケースを想定．(a)内部の図は，556 GHzのH_2O吸収線拡大図．木星大気の高速回転によって，吸収線の中心周波数がドップラーシフトをしている．